

---

# Dynamics of Agentic Loops in Large Language Models: A Geometric Theory of Trajectories

From Semantic Contraction to Exploratory Divergence

---

Nicolas Tacheny

University of Mons (Mons, Belgium)  
nicolas.tacheny@gmail.com

## Abstract

Agentic systems based on large language models operate through recursive feedback loops, where each output becomes the next input in an iterative transformation process. Understanding the geometric dynamics of these *agentic loops*, whether they converge, diverge or exhibit more complex behaviors, remains poorly characterized. This paper develops a geometric framework for analyzing agentic loop trajectories in semantic embedding spaces, treating iterative transformations as discrete dynamical systems.

We formalize the distinction between the *artifact space* (where linguistic transformations occur) and the *semantic embedding space* (where geometric measurements are performed). Since standard cosine similarities exhibit systematic bias due to embedding anisotropy, we introduce *calibrated similarity* using isotonic regression, which eliminates bias and improves correlation with human semantic judgments while maintaining high local stability. This calibrated metric enables precise geometric analysis through *trajectories* (temporal sequences of embeddings), *clusters* (regions of semantic coherence) and *attractors* (convergence points).

Experimentally, we characterize two fundamental *dynamical regimes* through singular agentic loops. A *contractive loop* performing iterative paraphrasing exhibits geometric convergence toward a stable attractor with decreasing dispersion. An *exploratory loop* alternating summarization and negation shows unbounded divergence with no stable clustering structure. These regimes demonstrate qualitatively distinct trajectory geometries, contraction versus expansion in semantic space.

Prompt design directly controls the dynamical regime, enabling systematic engineering of convergent versus divergent behaviors. This geometric framework provides the first rigorous quantitative approach to analyzing iterative transformation dynamics in LLMs, with applications to trajectory prediction, stability analysis and controlled composition of complex multi-step transformations.

## 1 Introduction

Large language models (LLMs) enable autonomous agentic systems that operate through recursive feedback loops, where each model output becomes the next input in an iterative transformation process. These *agentic loops* appear in diverse applications: iterative refinement systems that progressively improve outputs through self-critique, multi-step reasoning chains that decompose complex problems into intermediate steps and autonomous agents that maintain extended interactions with environments or users. Understanding the dynamics of these loops, whether they converge toward stable states, diverge unboundedly or exhibit complex oscillatory behaviors, remains poorly

characterized. Despite their increasing deployment in reasoning, planning and generation tasks, we lack a rigorous framework for analyzing how iterative transformations behave geometrically in semantic space.

Characterizing agentic loop dynamics has direct implications across multiple domains. For *system design*, knowing whether a loop exhibits convergent or divergent behavior enables engineers to select appropriate prompts and parameters for specific tasks, stable convergence is desirable for refinement and summarization, while controlled divergence may be useful for exploration and generation. For *reliability and safety*, detecting convergence properties helps identify runaway feedback loops that could produce unbounded drift or oscillation. For *theoretical understanding*, geometric trajectory analysis provides a quantitative lens for studying how language model transformations behave as discrete dynamical systems. The ability to predict, measure and control these dynamics is fundamental to deploying reliable iterative generative systems.

**Contributions.** The main contributions of this work are:

1. **A geometric framework for analyzing agentic loops.** We distinguish the artifact space (where text transformations occur) from the semantic embedding space (where geometric measurements are performed) and formalize how transformations induce measurable *trajectories*, temporal sequences of embeddings that trace the loop’s evolution through semantic space.
2. **A calibrated similarity metric.** To overcome the fundamental obstacle that pretrained embeddings exhibit anisotropy, concentrating cosine similarities around uninformative high values, we develop a calibrated metric using isotonic regression on human semantic judgments. This calibration eliminates bias and improves correlation while maintaining high local stability (98%), enabling precise trajectory analysis.
3. **The first systematic empirical characterization of dynamical regimes.** Through singular agentic loops, we identify and characterize two fundamental regimes: contractive convergence and exploratory divergence. We demonstrate that prompt design directly controls the geometric behavior of iterative transformations, establishing that agentic loop dynamics are predictable and controllable through prompt engineering.

The remainder of the paper is organized as follows. Section 2 reviews related work on iterative refinement, agentic systems, dynamical systems and embedding geometry. Sections 3–5 construct the geometric measurement infrastructure: embedding space construction, similarity calibration and stability validation. Section 6 formalizes the theoretical framework, defining agentic loops, trajectories, clusters, attractors and dynamical regimes. Section 7 presents experimental trajectory studies of contractive and exploratory singular loops, revealing fundamentally distinct geometric behaviors. Section 8 discusses implications for composite loops and controlled dynamics. Section 9 concludes.

An earlier version of this work was released as an arXiv preprint.

## 2 Related Work

**Computational creativity and the measurement problem.** The question of implementing computational creativity in iterative systems provides the broader motivation for this work. Boden [1] established the foundational framework for computational creativity, identifying three primary processes: **exploration** (searching conceptual spaces for new combinations), **transformation** (modifying the rules or structure of conceptual spaces) and **combination** (combining ideas from different domains). Colton and Wiggins [2] formalized creativity through measurable dimensions: **novelty** (semantic or structural distance from existing examples), **value** (quality, coherence and usefulness) and **surprise** (unexpectedness relative to prior expectations). Zhao et al. [3] recently demonstrated that large language models show creative behaviors across multiple tasks and domains.

These frameworks raise a fundamental question for iterative LLM systems: *How can we engineer agentic loops to implement Boden’s creative processes (explore-transform-combine) in ways that elevate Colton & Wiggins’ creativity metrics (novelty, value, surprise)?* Answering this question requires the ability to *measure* similarity-based metrics along trajectories, specifically to quantify

semantic distance (for novelty), coherence (for value) and discontinuities (for surprise) as iterative transformations unfold over time. However, computational creativity theory provides conceptual frameworks without addressing the foundational measurement infrastructure: *how do we rigorously measure semantic similarity and trajectory dynamics in embedding spaces?*

This measurement problem motivates our focus on geometric trajectory analysis as a necessary first step. Before we can engineer creative agentic loops or evaluate creativity metrics, we must establish rigorous methods for measuring similarity and characterizing trajectory dynamics. Our work addresses this foundational layer, building the geometric and dynamical measurement infrastructure required to eventually tackle computational creativity questions systematically.

Research on iterative generative systems has explored how large language models behave under recursive transformations, but geometric trajectory analysis of these dynamics remains underdeveloped. Beyond the creativity motivation, this work builds upon three main research threads: iterative refinement in language models, agentic systems and multi-step reasoning and embedding geometry.

**Iterative refinement in language models.** Madaan et al. [4] introduced Self-Refine, demonstrating that large language models can iteratively critique and improve their own outputs through a feedback loop without additional training. Their approach achieved substantial improvements across diverse tasks including dialogue generation and mathematical reasoning. However, Self-Refine focused on empirical task performance rather than analyzing the geometric structure of how representations evolve through iterations or characterizing convergence properties in semantic space.

Wei et al. [5] showed that chain-of-thought prompting enables large language models to perform complex reasoning by decomposing problems into intermediate steps. While this work established that prompting strategies significantly affect reasoning capabilities, it did not examine the stability or trajectory dynamics of iterative processes.

**Agentic systems and multi-step reasoning.** Recent work has explored how language models can act as autonomous agents through iterative interaction with environments or tools. Yao et al. [6] proposed ReAct, which interleaves reasoning traces with task-specific actions, enabling models to interact with external knowledge sources. Shinn et al. [7] introduced Reflexion, where agents use verbal reinforcement learning to maintain episodic memory and improve decision-making across trials. Park et al. [8] demonstrated generative agents that simulate believable human behavior through architectures combining memory, reflection and planning.

These agentic frameworks establish that recursive LLM interactions can produce sophisticated behaviors, but they do not formally characterize the dynamics of such systems in semantic space or analyze convergence and divergence patterns as geometric phenomena.

**Embedding geometry and semantic similarity.** Understanding the geometric structure of embedding spaces is crucial for analyzing semantic trajectories. Ethayarajh [9] systematically studied contextualized representations from BERT, ELMo and GPT-2, demonstrating that embeddings become increasingly anisotropic in upper layers, with vectors concentrating in a narrow cone. This anisotropy causes high cosine similarities even between semantically distant items, distorting similarity-based measurements.

Wang and Isola [10] analyzed contrastive representation learning through the lens of alignment (bringing similar items together) and uniformity (distributing representations across the hypersphere). They showed that good representations balance these competing objectives, providing theoretical grounding for why pretrained embeddings exhibit systematic geometric biases.

For calibrating similarity metrics, Niculescu-Mizil and Caruana [11] demonstrated that isotonic regression effectively transforms classifier scores into well-calibrated probabilities. While originally developed for classification tasks, isotonic regression provides a principled non-parametric method for aligning model outputs with empirical distributions. We extend this approach to semantic similarity calibration.

**Positioning of the present work.** In contrast to existing work, which primarily focuses on static properties of embeddings or isolated transformations, the present work studies the *dynamical*

*behavior* of iterative LLM transformations as geometric trajectories. Prior research on iterative refinement [4, 5] and agentic systems [6, 7, 8] has demonstrated impressive capabilities but treats each iteration as an independent step rather than as part of a continuous dynamical process. Similarly, embedding geometry research [9, 10] characterizes static distributional properties without examining how representations evolve under repeated transformations. Our work bridges these threads by treating agentic loops as discrete dynamical systems in semantic space, enabling the characterization of convergence, divergence and attractor structures through calibrated geometric measurements.

**Contribution of this work.** While computational creativity frameworks [1, 2] motivate the need to measure trajectory-based metrics, prior work has not developed the foundational geometric measurement infrastructure required to rigorously analyze iterative transformation dynamics. Self-refinement approaches [4] demonstrate empirical task improvements but do not characterize how representations evolve geometrically through iterations or analyze convergence versus divergence behaviors. Agentic frameworks [6, 7, 8] establish recursive LLM capabilities but lack quantitative measurement of trajectory dynamics in semantic space. Although embedding anisotropy is well-documented [9] and theoretical frameworks for representation quality exist [10], no existing work provides calibrated, human-aligned similarity metrics for rigorous trajectory analysis in iterative transformations.

**Our contribution builds the foundational geometric measurement infrastructure required for analyzing agentic loop dynamics, providing the tools necessary to eventually address computational creativity questions systematically.** We address these gaps through three main innovations. First, we develop a **geometric framework operating in the representation space** treating iterative transformations as discrete dynamical systems. This framework captures measurable trajectories, clusters, attractors and dynamical regimes that quantify how semantic representations evolve under recursive application. These geometric constructs open the path to provide to measure Colton & Wiggins’ creativity criteria. Second, we introduce **isotonic calibration that aligns embedding similarities with human semantic judgments** extending calibration methods [11] to overcome anisotropy [9] and enable precise geometric measurements using metrics that reflect human-perceived semantic distances. Third, we provide **systematic empirical characterization of dynamical regimes**. We demonstrate that prompt design directly determines whether agentic loops exhibit convergence, divergence or complex behaviors, as revealed by measurable geometric indicators in calibrated semantic space. This establishes the foundation for engineering Boden’s creative processes through controlled trajectory dynamics.

### 3 Semantic Space Construction

#### 3.1 Artifact Space

Before defining how we measure semantic dynamics, we must first specify what is being measured. In an agentic loop, the fundamental objects of transformation are *artifacts*: outputs generated and processed by a large language model. While artifacts can take various modalities (text, images, audio, code, etc.), in this paper we focus exclusively on **textual artifacts**.

We define the **artifact space**  $\mathcal{A}$  as the set of all possible text strings that can be generated by the language model. Each element  $a \in \mathcal{A}$  represents a complete textual output.

While  $\mathcal{A}$  is finite (bounded by the model’s vocabulary and maximum context length), it is combinatorially large and lacks inherent geometric structure suitable for quantitative analysis of convergence, divergence or semantic drift. To measure such dynamics, we construct a continuous representation space through embedding, as described in the following subsection.

#### 3.2 Representation Space and Embedding Function

To enable quantitative analysis of semantic dynamics, we construct a continuous **representation space**  $\mathcal{E}$  by embedding textual artifacts into a geometric space where distances and similarities can be measured.

Let  $\phi : \mathcal{A} \rightarrow \mathbb{R}^d$  denote an **embedding function** that maps each artifact  $a \in \mathcal{A}$  to a dense vector representation  $\phi(a) \in \mathbb{R}^d$  in a  $d$ -dimensional Euclidean space. To ensure that similarity

measurements depend solely on directional alignment (not magnitude), we apply  $\ell_2$ -normalization to all embeddings. Let  $\psi : \mathcal{A} \rightarrow \mathbb{S}^{d-1}$  denote the **normalized embedding function** defined as:

$$\psi(a) = \frac{\phi(a)}{\|\phi(a)\|_2}, \quad (1)$$

where  $\mathbb{S}^{d-1} = \{e \in \mathbb{R}^d : \|e\|_2 = 1\}$  is the  $(d - 1)$ -dimensional unit hypersphere. We define the **representation space** as:

$$\mathcal{E} = \{\psi(a) \mid a \in \mathcal{A}\} \subset \mathbb{S}^{d-1}. \quad (2)$$

Each artifact  $a$  is thus represented by a unit vector  $e = \psi(a) \in \mathcal{E}$ .

**Model-agnostic framework.** The framework presented above is **embedding-model agnostic**: any sentence encoder that maps text to dense vectors can instantiate  $\phi$  and our analysis of trajectories, clusters and dynamical regimes applies regardless of the specific model choice.

**Implementation choice.** For this work, we instantiate  $\phi$  using the `Xenova/paraphrase-mpnet-base-v2` model, a pretrained transformer encoder with  $d = 768$  dimensions. This model was chosen for three practical reasons:

1. It is trained on sentence pairs with human-labeled paraphrase relations, ensuring that geometric proximity corresponds to semantic similarity.
2. It offers a balanced trade-off between expressiveness and dimensionality, allowing fine-grained distinctions while remaining computationally efficient.
3. The `Xenova` implementation provides a reproducible and locally executable inference pipeline, facilitating controlled experimentation without external API dependencies.

The normalized representation space  $\mathcal{E} \subset \mathbb{S}^{767}$  thus forms the manifold on which all further measurements (distances, similarities and clustering) are defined.

### 3.3 Similarity Metric

Within the representation space  $\mathcal{E}$ , each artifact  $a \in \mathcal{A}$  is represented by its normalized embedding  $e = \psi(a) \in \mathcal{E} \subset \mathbb{S}^{d-1}$ . We define the model-based similarity function as

$$s^{(m)} : \mathbb{S}^{d-1} \times \mathbb{S}^{d-1} \rightarrow [-1, 1], \quad s^{(m)}(e_1, e_2) = \langle e_1, e_2 \rangle. \quad (3)$$

Since all elements of  $\mathcal{E}$  are unit vectors (i.e.,  $\|e\|_2 = 1$  for all  $e \in \mathcal{E}$ ), the inner product  $\langle e_1, e_2 \rangle$  directly equals the cosine of the angle between them, providing a normalized measure of semantic proximity.

In the following subsections, we first characterize the theoretical distribution of similarities in high-dimensional spaces (§3.4), then evaluate how well  $s^{(m)}$  aligns with human semantic judgments through quantitative metrics (§3.5) and visualization (§3.7).

### 3.4 High-Dimensional Similarity Distribution

On a standard high-dimensional unit sphere  $\mathbb{S}^{d-1}$ , two random vectors  $u, v$  drawn uniformly from the surface tend to be nearly orthogonal as the dimension increases. Formally, let  $X$  be uniformly distributed on  $\mathbb{S}^{d-1}$  and let  $f(X) = \langle X, v \rangle$  for a fixed  $v \in \mathbb{S}^{d-1}$ . By Lévy’s concentration inequality (see [12] for a modern treatment), for any  $t > 0$ ,

$$\mathbb{P}(|f(X) - \mathbb{E}[f(X)]| > t) \leq 2e^{-cnt^2}, \quad (4)$$

where  $c > 0$  is an absolute constant and  $n = d - 1$  is the dimension of the sphere. Since  $\mathbb{E}[f(X)] = 0$  for the uniform distribution, the inner product  $\langle u, v \rangle$  concentrates exponentially fast around 0 as  $d \rightarrow \infty$ . In such isotropic settings, the similarity distribution is symmetric and sharply peaked near zero.

However, the semantic embedding space induced by a pretrained language model such as `paraphrase-mpnet-base-v2` diverges from this theoretical isotropy. Because the model was trained on non-uniform pairs of semantically related sentences, the embeddings are not uniformly

distributed over the hypersphere but rather cluster around a dominant mean direction in  $\mathbb{R}^d$ . This induces a strong *anisotropy* of the embedding manifold, where most vectors share a large positive cosine with the mean embedding vector. As formalized by [10], good representation learning requires balancing two properties: *alignment* (similar points should be close) and *uniformity* (embeddings should be distributed uniformly on the unit sphere). The observed concentration violates the uniformity property, indicating that the pretrained model prioritizes alignment over uniform distribution. This trade-off is typical of contrastively trained embeddings. Empirically, the distribution of  $s^{(m)}(e_1, e_2)$  is concentrated around 0.8, in stark contrast with the isotropic baseline centered at 0.

### 3.5 Quantitative Metrics for Model-Human Alignment

To quantitatively assess how well  $s^{(m)}$  aligns with human semantic judgments, we use the **MTEB STS Benchmark (STS-train)** dataset. This dataset contains pairs of textual artifacts  $(a_1, a_2) \in \mathcal{A} \times \mathcal{A}$  annotated with normalized human similarity scores  $s^{(h)}(a_1, a_2) \in [0, 1]$ , rescaled from the original 0–5 range.

For each pair  $(a_1, a_2)$ , we compute their normalized embeddings  $e_1 = \psi(a_1)$  and  $e_2 = \psi(a_2)$  in the representation space  $\mathcal{E}$ . We then evaluate the model-based similarity  $s^{(m)}(e_1, e_2)$  and compare it to the human judgment  $s^{(h)}(a_1, a_2)$ .

We evaluate their alignment using complementary metrics, each capturing a distinct aspect of correlation or calibration:

- **Root Mean Squared Error (RMSE):**

$$\text{RMSE} = \sqrt{\frac{1}{N} \sum_{k=1}^N (s^{(m)}(e_1^k, e_2^k) - s^{(h)}(e_1^k, e_2^k))^2} \in [0, 1].$$

Measures the average magnitude of deviation between model and human similarities, penalizing large discrepancies more strongly. Lower RMSE indicates better agreement (RMSE = 0 means perfect match; RMSE = 1 indicates maximum deviation).

- **Mean Bias Error (MBE):**

$$\text{MBE} = \frac{1}{N} \sum_{k=1}^N (s^{(m)}(e_1^k, e_2^k) - s^{(h)}(e_1^k, e_2^k)) \in [-1, 1].$$

Quantifies systematic bias: positive when the model tends to overestimate human similarity, negative when it underestimates. MBE = 0 indicates no systematic bias;  $|\text{MBE}|$  close to 1 indicates severe consistent over- or under-estimation.

- **Expected Calibration Error (ECE):** This metric evaluates the degree to which model similarity scores are statistically calibrated to human perception. We partition the similarity range  $[0, 1]$  into  $B$  bins, where  $B_b$  denotes the set of sample pairs in bin  $b$ . For each bin, we compute:

- $\text{acc}(B_b)$ : the average human similarity score (*accuracy*, i.e., ground truth) within that bin
- $\text{conf}(B_b)$ : the average model similarity score (*confidence*, i.e., predicted value) within that bin

The ECE is then computed as the weighted average absolute deviation:

$$\text{ECE} = \sum_{b=1}^B \frac{|B_b|}{N} |\text{acc}(B_b) - \text{conf}(B_b)| \in [0, 1].$$

Lower ECE values indicate better calibration (ECE = 0 means perfect calibration; ECE = 1 indicates maximum miscalibration).

- **Pearson Correlation Coefficient ( $r$ ):**

$$r = \frac{\text{Cov}(s^{(m)}, s^{(h)})}{\sigma_{(m)} \sigma_{(h)}} \in [-1, 1],$$

where  $\text{Cov}(s^{(m)}, s^{(h)})$  is the covariance between model and human similarity scores,  $\sigma_{(m)}$  is the standard deviation of model scores and  $\sigma_{(h)}$  is the standard deviation of human scores. Explicitly, this can be computed as:

$$r = \frac{\sum_{k=1}^N (s_k^{(m)} - \bar{s}^{(m)})(s_k^{(h)} - \bar{s}^{(h)})}{\sqrt{\sum_{k=1}^N (s_k^{(m)} - \bar{s}^{(m)})^2} \sqrt{\sum_{k=1}^N (s_k^{(h)} - \bar{s}^{(h)})^2}},$$

where  $\bar{s}^{(m)}$  is the mean of model scores,  $\bar{s}^{(h)}$  is the mean of human scores and  $N$  is the total number of pairs. This metric captures the strength of *linear* dependence between model and human similarities.  $r = 1$  indicates perfect positive linear correlation,  $r = -1$  indicates perfect negative linear correlation and  $r = 0$  indicates no linear correlation. Values closer to  $\pm 1$  indicate stronger linear alignment.

- **Spearman Rank Correlation ( $\rho$ ):**

$$\rho = r_{\text{Pearson}}(\text{rank}(s^{(m)}), \text{rank}(s^{(h)})) \in [-1, 1],$$

where  $\text{rank}(s^{(m)})$  assigns each model similarity score its position when all  $N$  scores are sorted in ascending order and similarly for  $\text{rank}(s^{(h)})$ . The function  $r_{\text{Pearson}}(\cdot, \cdot)$  denotes the Pearson correlation coefficient applied to these rank vectors. This metric measures the *monotonic* alignment between the two orderings, independently of scale.  $\rho = 1$  indicates perfect monotonic agreement (rankings perfectly aligned),  $\rho = -1$  indicates perfect monotonic disagreement (rankings perfectly reversed) and  $\rho = 0$  indicates no monotonic relationship. Values closer to  $\pm 1$  indicate stronger monotonic alignment.

Quantitatively, the results obtained on the STS-train dataset are:

$$\text{RMSE} = 0.1702, \quad \text{MBE} = 0.0789, \quad \text{ECE} = 0.0797, \quad r = 0.8576, \quad \rho = 0.8430. \quad (5)$$

These metrics reveal several key properties of the embedding space. The **RMSE of 0.17** indicates a moderate average deviation between model and human similarities, suggesting reasonable overall agreement with some residual discrepancies. The **positive MBE of 0.079** shows a systematic tendency for the model to overestimate semantic similarity compared to human judgments. This is a characteristic feature of dense embedding spaces where related concepts cluster more tightly than human perception suggests. The **ECE of 0.080** quantifies the calibration gap: the model’s similarity scores are not perfectly aligned with the empirical frequency of human agreement, reflecting the need for recalibration to achieve probabilistic consistency. The **strong correlation values** ( $r = 0.86$  and  $\rho = 0.84$ ) confirm that despite these biases, the model captures the underlying rank order and linear structure of human semantic similarity judgments. Together, these results indicate that the embedding space preserves semantic relationships effectively while exhibiting systematic geometric biases, specifically anisotropic concentration of embeddings, that lead to consistent overestimation and miscalibration.

### 3.6 High-Confidence Similarity Threshold

To obtain a reliable decision boundary for semantic similarity, we introduce the **High-Confidence Similarity Threshold**  $\tau_{\text{HCS}}(s)$ , a data-driven value derived from human-judged highly similar pairs. This threshold provides a statistically principled criterion for determining when two sentences can be considered semantically similar with high confidence. Importantly, this concept is independent of any particular similarity measure and can be applied to any similarity function.

**Definition.** For a given similarity function  $s$  (such as the raw cosine similarity  $s^{(m)}$  or any other similarity function), the threshold is computed as:

$$\tau_{\text{HCS}}(s) = Q_{0.05}(s \mid s^{(h)} > 0.9) \quad (6)$$

that is, the 5% quantile of the similarity scores  $s$  among sentence pairs with high human similarity ( $s^{(h)} > 0.9$ ). The confidence level  $\alpha = 0.05$  is a standard choice, though it can be adjusted based on application requirements.

**Interpretation.** This definition is meaningful for three key reasons. First, the threshold is grounded in human judgments of semantic similarity rather than arbitrary choice. Second, it captures the lower bound of similarity scores for similar sentences as judged by humans. Third, it

provides a direct probabilistic guarantee: at least 95% of truly similar pairs (those with  $s^{(h)} > 0.9$ ) lie above this threshold.

**Statistical justification.** By construction, the threshold satisfies:

$$\mathbb{P}(s \geq \tau_{\text{HCS}}(s) \mid s^{(h)} > 0.9) \geq 0.95 \quad (7)$$

This conditional probability allows us to make reliable decisions: if a pair exceeds the threshold, it is likely to belong to the high-similarity group as defined by human raters.

**Decision criterion.** Any pair with similarity  $s \geq \tau_{\text{HCS}}(s)$  can be considered semantically similar with high confidence.

For the raw cosine similarity, we denote:

$$\tau_{\text{HCS}}^{(m)} = \tau_{\text{HCS}}(s^{(m)}) \approx 0.72 \quad (8)$$

### 3.7 Visualization of Similarity Distributions

Beyond these numerical indicators, we visualize the distributions and relationships between  $s^{(m)}$  and  $s^{(h)}$  using density estimation techniques.

To compare model similarities with human similarity judgments, we estimate their respective continuous distributions using *Kernel Density Estimation (KDE)*. Each observed value contributes a Gaussian “bump” to the overall density, producing a smooth, non-parametric approximation of the underlying probability function:

$$\hat{f}_h(x) = \frac{1}{nh\sqrt{2\pi}} \sum_{i=1}^n e^{-\frac{1}{2}\left(\frac{x-x_i}{h}\right)^2}, \quad h = 1.06 \hat{\sigma} n^{-1/5}. \quad (9)$$

Silverman’s rule [13] selects the optimal bandwidth  $h$ , balancing smoothness and resolution. We compute separate densities for human scores and model similarities,  $\hat{f}_H(x)$  and  $\hat{f}_S(x)$  and plot them over  $[0, 1]$ . Alignment between both curves indicates good agreement, while systematic shifts reveal under- or over-confidence in the model’s similarity predictions. Additionally, both visualizations include a vertical green line marking the high-confidence similarity threshold  $\tau_{\text{HCS}}^{(m)}$  (defined in §3.6), which serves as a data-driven decision boundary for determining when two sentences can be considered semantically similar with high confidence.

In addition to that, we also compute joint density heatmaps. To evaluate the relationship between human similarity judgments and model predictions, we estimate their joint density over the  $[0, 1]^2$  space. The domain is divided into a regular grid of bins and each cell’s density  $\rho_{ij} = N_{ij}/(n \Delta x \Delta y)$  reflects the concentration of pairs  $(h_i, s_i)$ . A 2D Gaussian smoothing kernel can be applied to obtain a continuous density field  $\tilde{\rho}(x, y)$ , from which iso-density contours and a color intensity map are derived. The diagonal  $y = x$  represents perfect alignment, where model similarities equal human scores. High density concentrated along this diagonal indicates strong agreement, while systematic deviations above or below it reveal over- or under-confidence and vertical dispersion signals inconsistency in the model’s predictions.

Figure 1a reveals a striking concentration of model similarities around 0.8, contrasting sharply with the broader distribution of human scores across  $[0, 1]$ . This concentration reflects the anisotropic geometry of the embedding space, where semantically related sentences cluster tightly on the unit hypersphere, violating the theoretical isotropy assumption. The green vertical line at  $\tau_{\text{HCS}}^{(m)}$  marks the decision boundary derived from high-confidence human judgments, positioned within this concentration region, indicating that most model similarities for genuinely similar pairs fall within this narrow band. Human judgments, by contrast, exhibit greater variability, with substantial density in the low-to-moderate similarity range  $([0.2, 0.6])$ , indicating more nuanced perceptual distinctions.

Figure 1b visualizes the joint density  $\tilde{\rho}(s^{(h)}, s^{(m)})$  as a 2D heatmap. The density mass lies predominantly above the diagonal  $y = x$ , confirming systematic overestimation: the model assigns higher similarity scores than humans across most pairs. The vertical spread for human scores in the range  $[0.3, 0.7]$  indicates high variance in model predictions for pairs with intermediate human similarity: the model struggles to distinguish subtle semantic differences, compressing them into

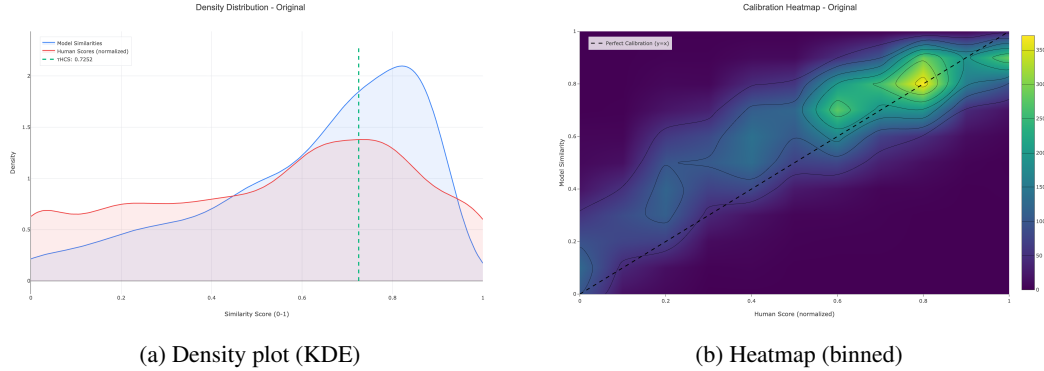


Figure 1: Original (uncalibrated) cosine similarity versus human similarity scores.

a narrow band around 0.8. In contrast, pairs with very low human similarity ( $s^{(h)} < 0.3$ ) show tighter correspondence, suggesting the model correctly identifies dissimilar pairs but struggles to capture gradations of relatedness.

These visualizations expose a fundamental calibration gap: the model’s cosine similarity  $s^{(m)}(e_1, e_2)$  does not align with human semantic judgments  $s^{(h)}(e_1, e_2)$ , both in terms of distribution shape (concentration vs. spread) and pointwise correspondence (systematic overestimation). This raises a natural question: *Can we recalibrate or transform the model’s similarity function to improve its correlation with human semantic judgments?* This question is investigated in the following section.

## 4 Calibration of Semantic Similarity

The visualizations in Section 3.7 reveal systematic bias in the model’s similarity predictions:  $s^{(m)}$  consistently overestimates human judgments  $s^{(h)}$  and exhibits compressed variance. Calibration provides a post-processing mechanism to correct these distributional and pointwise misalignments.

Formally, calibration seeks a transformation function  $g : [-1, 1] \rightarrow \mathbb{R}$  such that the calibrated similarity

$$\tilde{s}(e_1, e_2) = g(s^{(m)}(e_1, e_2)) \quad (10)$$

better aligns with human similarity judgments  $s^{(h)}(e_1, e_2)$ .

### 4.1 Overview of Calibration Methods

We evaluate several calibration functions that map cosine similarity to human-aligned scores, each varying in parametric flexibility and nonlinearity.

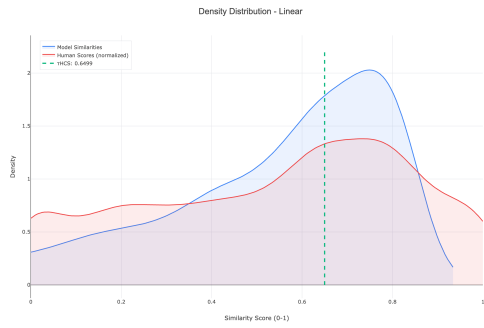
**Linear regression** fits a simple affine transformation  $\tilde{s}(x) = ax + b$ , providing a global scaling and shift but unable to capture nonlinear patterns (Figure 2).

**Isotonic regression** learns a monotonic, piecewise-constant mapping that adapts locally to the data without assuming a functional form, allowing flexible nonlinear calibration while preserving rank ordering (Figure 3).

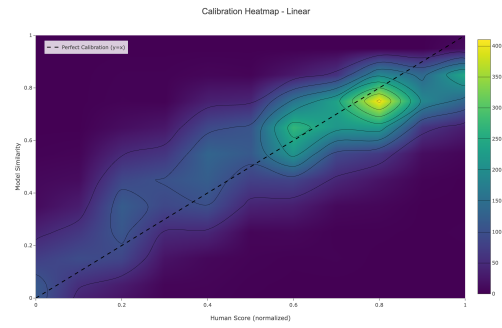
**Sigmoid mapping** applies a logistic curve  $\tilde{s}(x) = 1/(1 + e^{-a(x-b)})$ , modeling smooth saturation at similarity extremes (Figure 4).

**Polynomial transformations** (degrees 2, 3 and 4) fit  $\tilde{s}(x) = \sum_{i=0}^n a_i x^i$ , offering increasing flexibility to model curvature, though higher degrees may introduce unwanted oscillations (Figures 5, 6, 7).

**Beta distribution calibration** uses a beta CDF parameterized by shape  $\alpha$  and  $\beta$ , suited for bounded, skewed distributions but prone to instability when assumptions mismatch the data (Figure 8).

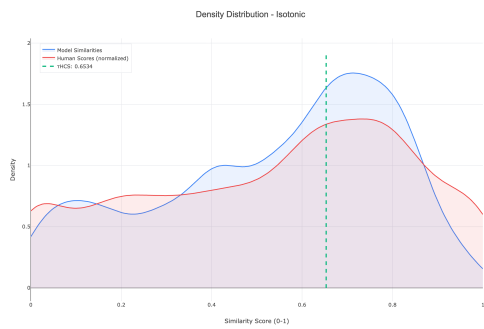


(a) Density plot (KDE)

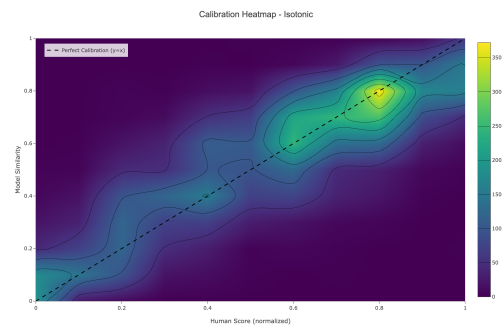


(b) Heatmap (binned)

Figure 2: Linear regression calibration.

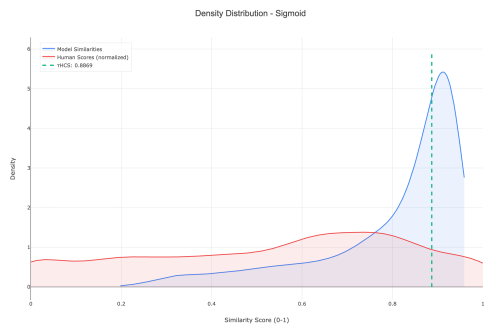


(a) Density plot (KDE)

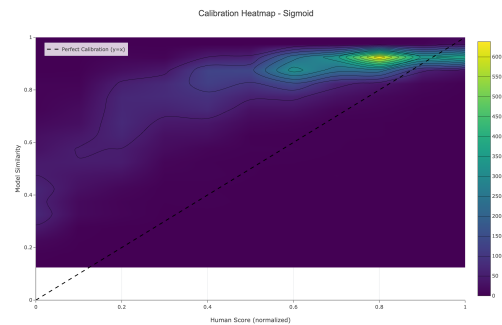


(b) Heatmap (binned)

Figure 3: Isotonic regression calibration.

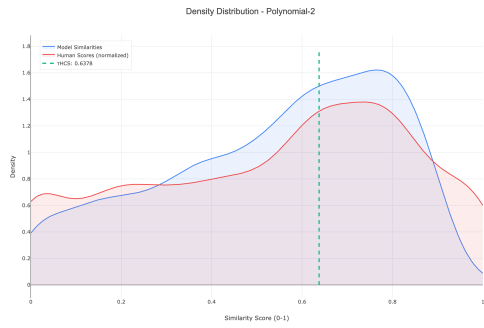


(a) Density plot (KDE)

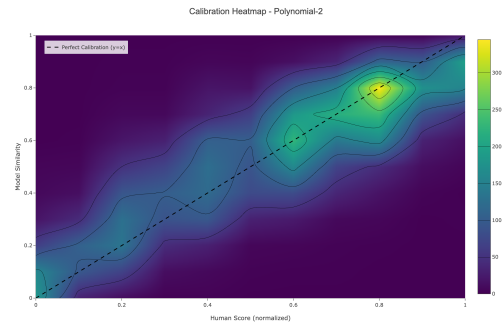


(b) Heatmap (binned)

Figure 4: Sigmoid calibration.

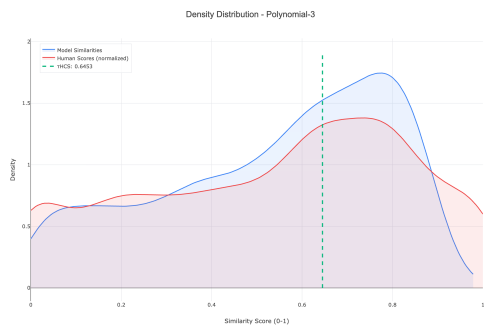


(a) Density plot (KDE)

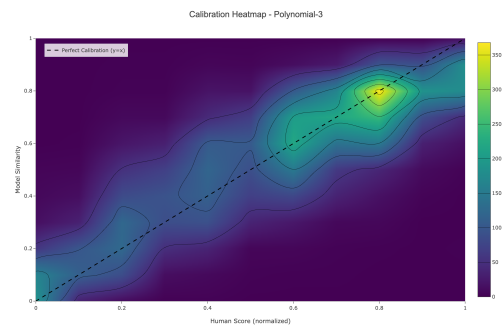


(b) Heatmap (binned)

Figure 5: Polynomial degree 2 calibration.

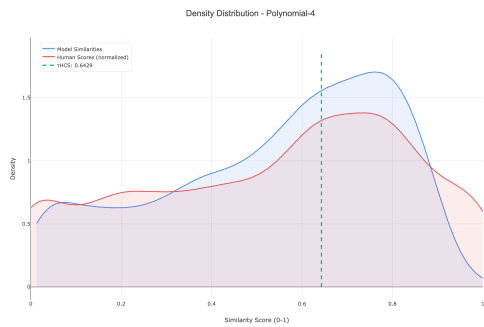


(a) Density plot (KDE)

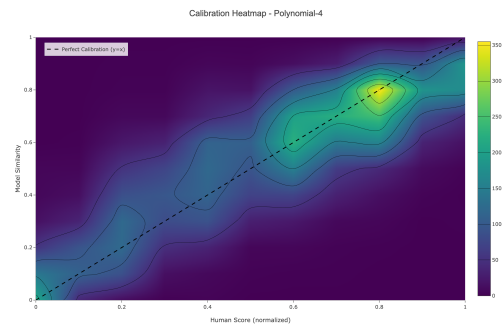


(b) Heatmap (binned)

Figure 6: Polynomial degree 3 calibration.



(a) Density plot (KDE)



(b) Heatmap (binned)

Figure 7: Polynomial degree 4 calibration.

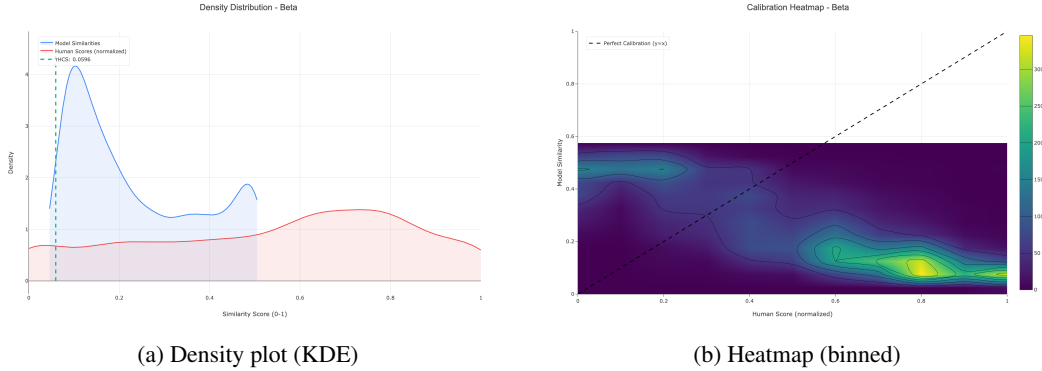


Figure 8: Beta distribution calibration.

## 4.2 Results

Table 1 presents the performance comparison of all calibration methods against the original (un-calibrated) cosine similarity using correlation metrics. Percentage changes relative to the original baseline are shown for reference.

Method	RMSE	MBE	ECE	Pearson $r$	Spearman $\rho$
Original	0.1702	0.0789	0.0797	0.8576	0.8430
Linear	0.1506 ↓11.5%	0.0000 ↓100.0%	0.0222 ↓72.1%	0.8576 ±0.0%	0.8430 ±0.0%
<b>Isotonic</b>	<b>0.1411 ↓17.1%</b>	<b>0.0000 ↓100.0%</b>	<b>0.0000 ↓99.9%</b>	<b>0.8764 ↑2.2%</b>	<b>0.8563 ↑1.6%</b>
Sigmoid	0.3192 ↑87.6%	0.2604 ↑230.2%	0.2604 ↑226.7%	0.8182 ↓4.6%	0.8430 ±0.0%
Beta	0.5168 ↑203.6%	-0.3011 ↑281.8%	0.4243 ↑432.3%	-0.8266 ↓196.4%	-0.8246 ↓197.8%
Polynomial-2	0.1474 ↓13.4%	0.0004 ↓99.5%	0.0095 ↓88.1%	0.8641 ↑0.8%	0.8430 ±0.0%
Polynomial-3	0.1472 ↓13.5%	0.0000 ↓100.0%	0.0057 ↓92.8%	0.8644 ↑0.8%	0.8430 ±0.0%
Polynomial-4	0.1472 ↓13.5%	-0.0000 ↓100.0%	0.0058 ↓92.7%	0.8645 ↑0.8%	0.8430 ±0.0%

Table 1: Performance comparison of calibration methods with percentage changes relative to the original baseline. For RMSE, MBE and ECE, lower is better (green ↓); for Pearson and Spearman, higher is better (green ↑).

Isotonic regression achieves the strongest monotonic correlation (Spearman  $\rho = 0.8563$ ) and lowest calibration error (ECE = 0.0000), with perfect elimination of mean bias (MBE = 0.0000) and a 17.1% reduction in RMSE compared to the original baseline. This defines our *calibrated similarity function*

$$\tilde{s} : \mathbb{S}^{d-1} \times \mathbb{S}^{d-1} \rightarrow \mathbb{R}, \quad \tilde{s} = f_{\text{isotonic}} \circ s^{(m)} \quad (11)$$

used throughout the dynamic analysis. In practice, since we align with human similarity scores in  $[0, 1]$ , calibrated outputs are clamped to this interval.

Similarly, we define the high-confidence similarity threshold for the calibrated similarity:

$$\tilde{\tau}_{\text{HCS}} = \tau_{\text{HCS}}(\tilde{s}) \approx 0.65 \quad (12)$$

## 5 Evaluating Local Stability of the Semantic Space

### 5.1 Motivation

Even if the calibrated semantic similarity aligns well with human judgments, it remains essential to evaluate the *local stability* of the embedding function  $\psi : \mathcal{A} \rightarrow \mathcal{E}$  itself. A locally stable embedding function should preserve high similarity under small linguistic perturbations: when two texts differ only slightly in form or syntax, their semantic similarity should remain consistently high. However,  $\psi$  is learned and discretized; neither its continuity nor its Lipschitz properties can be guaranteed theoretically. Our first objective is therefore empirical: to determine whether  $\psi$  behaves as *locally stable* in practice.

However, a critical methodological concern arises from our use of isotonic regression for calibration. While isotonic regression optimally preserves monotonicity and eliminates bias, it produces a *piecewise constant* (and therefore discontinuous) mapping  $f_{\text{isotonic}}$ . This raises an essential question: **does the discontinuous nature of isotonic regression degrade the local stability observed in the raw embedding space?**

To address both concerns, we conduct a dual analysis of stability:

1. **Base model stability**, evaluated on raw cosine similarity  $s^{(m)}$ , measures how the uncalibrated embedding function reacts to small linguistic perturbations.
2. **Calibrated stability**, evaluated on the calibrated similarity  $\tilde{s}$ , measures whether isotonic calibration preserves or degrades this local stability.

Comparing these two perspectives allows us to validate that calibration does not introduce artificial instabilities, ensuring that the semantic trajectories observed in agentic loops reflect genuine semantic dynamics rather than artifacts of the calibration process.

## 5.2 Artifact Perturbation Definition

To evaluate local stability, we constructed a dedicated dataset using ChatGPT to generate pairs of sentences differing by minimal and controlled linguistic perturbations. Each pair  $(a_i, a'_i)$  was manually categorized into one of seven perturbation types, each intended to simulate a semantically minimal transformation while introducing specific syntactic or lexical variations. This approach allows for systematic testing of  $\psi$ 's local stability across controlled linguistic dimensions.

The following perturbation types were included, each illustrated with examples from the dataset:

- **DETERMINER\_VARIATION:** A minimal change affecting only the determiner (the, a, this, that) without modifying the tense, structure or semantic content of the sentence. *Example:* "The cat sleeps on the sofa." → "A cat sleeps on the sofa."
- **TENSE\_VARIATION:** A transformation that shifts the verbal tense while preserving the event described by the sentence. *Example:* "She drinks tea in the morning." → "She drank tea in the morning."
- **SYNONYM\_SUBSTITUTION:** Replacing a lexical item (noun, verb, adjective) with a close synonym that preserves the meaning. *Example:* "He reads a book every night." → "He reads a novel every night."
- **LOGICAL\_PARAPHRASE:** A reformulation that preserves the logical meaning of the sentence, often through active/passive alternation or structural inversion. *Example:* "The teacher explains the lesson." → "The lesson is explained by the teacher."
- **NOMINALIZATION:** Transforming a predicate into its nominal form (or the reverse) while keeping the meaning equivalent. *Example:* "He decided to leave early." → "He made a decision to leave early."
- **COREFERENCE\_EXPANSION:** Replacing a pronoun with its explicit referent (or vice versa), keeping the propositional content unchanged. *Example:* "Alice lost her keys." → "Alice lost Alice's keys."
- **QUANTIFIER\_VARIATION:** Replacing a quantifier with another logically equivalent form (all  $\leftrightarrow$  every), without changing the truth conditions. *Example:* "All cats like to sleep." → "Every cat likes to sleep."

The dataset comprises 700 pairs across all categories (100 pairs per type), covering both lexical and syntactic variations. This controlled diversity allows us to examine how different perturbation types affect similarity in both the raw and calibrated embedding spaces.

## 5.3 Metrics and Methodology

For each pair  $(a_i, a'_i)$ , we compute their normalized embeddings  $e_i = \psi(a_i)$  and  $e'_i = \psi(a'_i)$  within  $\mathbb{S}^{d-1}$ . We then measure stability using two complementary similarity functions:

**Base model similarity.** We compute the raw cosine similarity:

$$s_i^{(m)} = s^{(m)}(e_i, e'_i) = \langle e_i, e'_i \rangle, \quad (13)$$

which measures the uncalibrated similarity between perturbed pairs.

**Calibrated similarity.** We also compute the calibrated similarity:

$$\tilde{s}_i = \tilde{s}(e_i, e'_i) = f_{\text{isotonic}}(s_i^{(m)}), \quad (14)$$

where  $f_{\text{isotonic}}$  denotes the isotonic regression mapping introduced in Section 4.

For each perturbation type  $k$  with  $N_k$  pairs, we compute three stability indicators:

$$\mu_k = \frac{1}{N_k} \sum_{i \in \mathcal{I}_k} s_i, \quad \sigma_k = \sqrt{\frac{1}{N_k} \sum_{i \in \mathcal{I}_k} (s_i - \mu_k)^2}, \quad r_k = \frac{1}{N_k} \sum_{i \in \mathcal{I}_k} \mathbf{1}_{\{s_i \geq \tau\}}, \quad (15)$$

where  $\mathcal{I}_k$  denotes the index set of pairs for perturbation type  $k$  and  $\tau$  is the stability threshold.

**Threshold selection.** Rather than choosing arbitrary thresholds, we use the data-driven high-confidence similarity thresholds defined in Section 3.6:

- For base model similarity:  $\tau = \tau_{\text{HCS}}^{(m)} \approx 0.72$
- For calibrated similarity:  $\tau = \tilde{\tau}_{\text{HCS}} \approx 0.65$

The stability rate  $r_k$  thus measures the proportion of perturbed pairs that maintain similarity above the threshold derived from high-confidence human judgments, providing a principled criterion for local stability.

## 5.4 Empirical Results

Tables 2 and 3 report the local stability metrics for base model (raw cosine) and calibrated similarities, respectively. For each perturbation type, we provide the number of pairs, mean similarity, standard deviation and stability rate (proportion of pairs exceeding the corresponding threshold).

Perturbation Type	Pairs ( $N_i$ )	Mean ( $\mu_{\text{base},i}$ )	Std. Dev. ( $\sigma_{\text{base},i}$ )	Stab. Rate ( $r_{\text{base},i}$ )
DETERMINER VARIATION	100	0.932	0.017	1.00
TENSE VARIATION	100	0.909	0.030	1.00
SYNONYM SUBSTITUTION	100	0.853	0.060	0.95
LOGICAL PARAPHRASE	100	0.891	0.023	1.00
NOMINALIZATION	100	0.866	0.035	1.00
COREFERENCE EXPANSION	100	0.882	0.022	1.00
QUANTIFIER VARIATION	100	0.848	0.039	0.97
<b>All types (overall)</b>	<b>700</b>	<b>0.883</b>	<b>0.045</b>	<b>0.99</b>

Table 2: Local stability metrics using base model similarity  $s^{(m)}$  (threshold  $\tau_{\text{HCS}}^{(m)} = 0.72$ ).

Perturbation Type	Pairs ( $N_i$ )	Mean ( $\mu_{\text{sim},i}$ )	Std. Dev. ( $\sigma_{\text{sim},i}$ )	Stab. Rate ( $r_{\text{sim},i}$ )
DETERMINER VARIATION	100	0.926	0.054	1.00
TENSE VARIATION	100	0.868	0.069	1.00
SYNONYM SUBSTITUTION	100	0.799	0.082	0.87
LOGICAL PARAPHRASE	100	0.831	0.049	1.00
NOMINALIZATION	100	0.818	0.078	1.00
COREFERENCE EXPANSION	100	0.830	0.045	1.00
QUANTIFIER VARIATION	100	0.798	0.050	0.97
<b>All types (overall)</b>	<b>700</b>	<b>0.839</b>	<b>0.075</b>	<b>0.98</b>

Table 3: Local stability metrics using calibrated similarity  $\tilde{s}$  (threshold  $\tilde{\tau}_{\text{HCS}} = 0.65$ ).

## 5.5 Discussion

The comparison between Tables 2 and 3 reveals two critical findings regarding local stability.

**Embedding function exhibits strong local stability.** The base model similarity analysis (Table 2) demonstrates that the embedding function  $\psi$  exhibits excellent local stability, with an overall stability rate of 99%. All perturbation types maintain mean similarities well above the threshold  $\tau_{\text{HCS}}^{(m)} = 0.72$ , ranging from 0.848 (QUANTIFIER\_VARIATION) to 0.932 (DETERMINER\_VARIATION). This confirms that the pretrained embedding model is robust to small linguistic perturbations, preserving high semantic similarity even under controlled transformations such as tense variation, synonym substitution and logical paraphrasing.

**Isotonic calibration introduces minimal stability degradation.** Table 3 shows that isotonic regression calibration slightly reduces the overall stability rate from 99% to 98%, a modest degradation of only 1 percentage point. This small decrease is attributable to the *piecewise constant* (discontinuous) nature of isotonic regression: when a perturbed pair  $(a_i, a'_i)$  has a raw cosine similarity  $s^{(m)}$  near a discontinuity point of  $f_{\text{isotonic}}$ , the calibrated similarities  $\tilde{s}(e_i, e_i)$  and  $\tilde{s}(e'_i, e'_i)$  may fall into different constant segments, potentially crossing the threshold  $\tilde{\tau}_{\text{HCS}} = 0.65$ .

The most affected perturbation type is SYNONYM\_SUBSTITUTION, whose stability rate drops from 0.95 to 0.87. This is expected: synonym substitutions produce moderate cosine similarities (mean 0.853) that fall in a region where isotonic regression has more step discontinuities. In this moderate range, small linguistic perturbations can cause similarities to jump across step boundaries in  $f_{\text{isotonic}}$ , leading to larger changes in calibrated values than in the original cosine similarities. Conversely, perturbation types with very high base similarities (TENSE\_VARIATION: 0.909, DETERMINER\_VARIATION: 0.932) remain perfectly stable ( $r = 1.00$ ) after calibration, as their similarities fall in a region where isotonic regression is nearly constant and far from the threshold.

**Practical acceptability of calibrated stability.** Despite the theoretical discontinuity of isotonic regression, the empirical stability rate of 98% remains *highly acceptable* for practical use. This demonstrates that isotonic regression achieves its primary goal (eliminating bias and improving correlation with human judgments) without substantially compromising local stability. The 1% degradation is a negligible cost compared to the significant gains in calibration quality (ECE reduction from 0.0797 to 0.0000, as shown in Table 1).

**Implications for dynamic analysis.** These results validate the use of calibrated similarity  $\tilde{s}$  for studying agentic loop dynamics. The embedding function  $\psi$  exhibits strong local stability and isotonic calibration preserves this property with only minimal degradation. This ensures that the semantic trajectories observed in agentic loops reflect genuine semantic evolution rather than instabilities introduced by either the embedding function or the calibration process. With local stability empirically established, we now turn to the formal analysis of *agentic loop dynamics*, confident that our similarity metric provides a stable and human-aligned foundation for measuring iterative transformations in generative systems.

## 6 Agentic Loop Dynamics: Theoretical Framework

This section formalizes the theoretical framework underlying agentic loop dynamics, defining key concepts such as trajectory, cluster and attractor before turning to empirical experiments.

### 6.1 Foundational Spaces and Operations

We begin by establishing the mathematical spaces and primitive operations that underlie all agentic loop structures.

**Artifact and embedding spaces.** Let  $\mathcal{A}$  denote the *artifact space*, where each element  $a \in \mathcal{A}$  represents a linguistic artifact (e.g., a sentence, paragraph or document). Let  $\psi : \mathcal{A} \rightarrow \mathcal{E}$  be the embedding map introduced in Section 3, which projects artifacts into a semantic vector space where their meaning can be quantitatively compared.

**Primitive operations.** We introduce two fundamental operations:

- $\text{LLM} : \mathcal{A} \rightarrow \mathcal{A}$  denotes a large language model’s generation operation, which takes a formatted input string (prompt) and produces a generated output string. The same underlying model may be invoked with different generation parameters (temperature  $T$ , top-p, top-k, seed, etc.), which we denote as  $\text{LLM}_\theta$  where  $\theta$  represents the parameter configuration.
- $P : \mathcal{A} \rightarrow \mathcal{A}$  denotes a *prompt template*, a function that embeds an artifact  $a \in \mathcal{A}$  into a formatted prompt string suitable for LLM consumption. For example,  $P(a) =$  “Rewrite the following:  $\{a\}$ ” structures the artifact within an instruction.

### 6.2 Agentic Loops and Trajectories

**Agentic Loop.** An *agentic loop* is a discrete dynamical system  $(\mathcal{A}, F)$  where  $F : \mathcal{A} \rightarrow \mathcal{A}$  is a transformation operator that defines the recursive rule generating the sequence:

$$a_{t+1} = F(a_t), \quad t \in \mathbb{N}, \quad \text{with initial condition } a_0 \in \mathcal{A}. \quad (16)$$

Using the primitive operations defined above,  $F$  is implemented as:

$$F(a_t) = \text{LLM}(P(a_t)). \quad (17)$$

Each iteration produces a new artifact  $a_{t+1}$  from the previous artifact  $a_t$  through this composition of prompt template and LLM generation, starting from an initial artifact  $a_0$ . The corresponding representations in the embedding space  $\mathcal{E}$  evolve as:

$$e_t = \psi(a_t), \quad e_{t+1} = \psi(a_{t+1}) = \psi(\text{LLM}(P(a_t))), \quad \text{with } e_0 = \psi(a_0). \quad (18)$$

The resulting sequence  $\{e_t\}_{t=0}^T$  allows us to track the evolution of the loop dynamics in the continuous embedding space  $\mathcal{E}$ , where we can quantitatively measure distances and similarities between successive states.

We distinguish three types of agentic loops based on the structure of  $F$ :

1. **Singular loop:**  $F = \text{LLM} \circ P$  where  $P$  is a single prompt template. Each iteration applies one LLM call:  $a_{t+1} = \text{LLM}(P(a_t))$ . This is the focus of our empirical study (Section 7).
2. **Composite loop:**  $F = \text{LLM}_n \circ P_n \circ \dots \circ \text{LLM}_1 \circ P_1$  where each  $(P_i, \text{LLM}_i)$  pair represents a distinct transformation phase. Here,  $\text{LLM}_i$  denotes an LLM invocation with specific generation parameters (temperature, top-p, seed, etc.), which may differ across phases to induce different behaviors, for instance high temperature for creative exploration, low temperature for precise consolidation. Different model architectures can also be used (e.g., specialized models for critique vs. generation). For example, generate-critique-revise requires three sequential LLM calls with different prompt templates and potentially different sampling configurations. Composite loops enable controlled creativity through role-based phase alternation (Section 8.4).
3. **Graph based loop:**  $F$  is derived from a directed acyclic computation graph that could include parallel execution and conditional branches, forming the basis for multi-agent architectures (Section 8.5).

This paper establishes the theoretical framework applicable to all three types, then focuses empirically on *singular loops* to rigorously characterize fundamental dynamical regimes. Understanding singular loop behavior provides the necessary foundation for analyzing composite and graph based loops in future work.

**Agentic Trajectory.** The iterative process produces an ordered sequence of embedded representations:

$$\mathcal{T} = \{e_t = \psi(a_t) \mid t = 0, 1, \dots, T\} \subset \mathcal{E}, \quad (19)$$

which we call the *agentic trajectory*. Each transition  $(e_t, e_{t+1})$  represents a local semantic displacement, whose magnitude and direction quantify the instantaneous dynamics of the loop.

### 6.3 Semantic Geometry of Trajectories

Having defined how trajectories are generated, we now introduce geometric tools to measure their structure. When a trajectory exhibits temporal stability, meaning embeddings remain close to each other for an extended period, we need mathematical concepts to characterize this clustering behavior.

**Center of Gravity.** Given a set of embeddings  $E = \{e_{i_1}, e_{i_2}, \dots, e_{i_k}\} \subset \mathcal{E}$ , the *center of gravity*  $a_E$  is defined as the  $L^2$ -normalized mean:

$$a_E = \frac{\mu_E}{\|\mu_E\|_2}, \quad \text{where} \quad \mu_E = \frac{1}{k} \sum_{j=1}^k e_{i_j}. \quad (20)$$

The center of gravity minimizes the sum of squared Euclidean distances to all embeddings in  $E$  and is itself a unit vector:  $\|a_E\|_2 = 1$ . This provides a natural reference point for measuring how tightly a set of embeddings is concentrated.

**Semantic Dispersion.** To quantify this concentration, we define the *semantic dispersion*, which measures the maximum deviation from the center in calibrated similarity space:

$$\text{Dispersion}(E) = \max_{e \in E} [1 - \tilde{s}(e, a_E)], \quad (21)$$

where  $\tilde{s}$  is the calibrated similarity function from Section 4. Smaller dispersion indicates tighter semantic coherence;  $\text{Dispersion}(E) = 0$  means all embeddings are semantically identical to the center of gravity. Together, the center of gravity and dispersion allow us to characterize when a trajectory remains in a stable semantic region.

### 6.4 Clusters and Attractors

Armed with these geometric tools, we can now formalize the notion of a *cluster*, a contiguous temporal segment where the trajectory maintains semantic stability.

**Cluster.** A *cluster*  $C \subseteq \mathcal{T}$  is a maximal contiguous temporal window  $[t_a, t_b]$  of the agentic trajectory where embeddings maintain semantic coherence, up to a set of outliers  $O_C$ :

$$C = \{e_t \mid t \in [t_a, t_b] \setminus O_C\} \quad \text{with center of gravity} \quad a_C = \frac{\sum_{e \in C} e}{\|\sum_{e \in C} e\|_2}. \quad (22)$$

The cluster represents a phase during which the loop operates within a bounded semantic region, repeatedly generating artifacts with similar meanings.

**Cluster Validity Constraints.** Not every temporal window qualifies as a cluster. To ensure semantic coherence, a cluster must satisfy three validity constraints:

1. **Similarity ( $\lambda$ ):** For all  $t \in [t_a + 1, t_b] \setminus O_C$ ,  $\tilde{s}(e_{t-1}, e_t) \geq \lambda$ , ensuring consecutive embeddings remain semantically close
2. **Dispersion ( $\rho$ ):**  $\text{Dispersion}(C) < \rho$ , ensuring the cluster as a whole stays tightly concentrated

3. **Patience ( $\kappa$ ):** At most  $\kappa$  consecutive violations allowed before cluster termination, allowing temporary noise

Parameters:  $\lambda \in [0, 1]$  (local coherence),  $\rho > 0$  (global coherence),  $\kappa \in \mathbb{N}$  (noise tolerance). These constraints maintain semantic coherence while allowing for occasional outliers.

**Attractor.** For a cluster  $C$  with center of gravity  $a_C$ , the *attractor* is simply  $a_C$ , the semantic region toward which the trajectory converges during  $C$ 's temporal extent. This terminology borrows from dynamical systems theory: the attractor represents the "pull" that keeps the trajectory within a stable semantic basin.

## 6.5 Dynamic Regimes

Finally, we characterize the global behavior of agentic loops by categorizing the qualitative patterns their trajectories exhibit over time.

**Classification.** An agentic loop's dynamics fall into one of three regimes:

- **Contractive ( $\mathcal{R}_{\text{ctr}}$ ):** There exists a time  $T$  such that for all  $t \geq T$ , the trajectory remains within a single cluster. The loop stabilizes around a coherent semantic region.
- **Oscillatory ( $\mathcal{R}_{\text{osc}}$ ):** The trajectory alternates among a finite set of recurrent clusters without converging to one. The loop cycles through distinct semantic regions.
- **Exploratory ( $\mathcal{R}_{\text{exp}}$ ):** The trajectory exhibits unbounded or aperiodic movement within  $\mathcal{E}$ , showing no stable attractor. The loop continuously generates novel semantic content without stabilization.

These categories provide a conceptual basis for describing the emergent behavior of agentic loops and for distinguishing structured evolution from uncontrolled semantic drift.

**Scope and operationalization.** The formal definitions provided above serve as conceptual anchors for the mathematical framework. In our empirical analysis (Section 7), we use operational approximations rather than computing exact topological limits. This pragmatic approach allows us to identify and characterize emergent structures within finite-sample trajectories while remaining grounded in the theoretical principles outlined above.

Note that the *Oscillatory Regime* (periodic cycling among multiple attractors) is not observed in our experiments (Section 7). The prompts we designed exhibit either full convergence (Contractive) or complete divergence (Exploratory), with no sustained oscillation between distinct semantic regions. Exploring conditions that produce oscillatory dynamics, such as prompts with explicit alternating instructions or adversarial constraints, remains an avenue for future work.

## 6.6 Cluster Detection Algorithm

To operationalize the cluster and attractor definitions presented in Section 6.4, we employ an *incremental cluster detection algorithm* that processes the trajectory  $\{e_t\}_{t=0}^T$  sequentially, identifying stable regions where embeddings maintain semantic coherence around a common center of gravity. The algorithm implements the validity constraints defined earlier using three parameters: similarity threshold  $\lambda \in [0, 1]$ , dispersion threshold  $\rho > 0$  and patience  $\kappa \in \mathbb{N}$ .

**Detection procedure.** The algorithm processes embeddings sequentially and maintains a candidate cluster. At each iteration  $t$ , it evaluates the cluster validity constraints:

- (i) **Similarity:** consecutive embeddings satisfy  $\bar{s}(e_{t-1}, e_t) \geq \lambda$ ;
- (ii) **Dispersion:** adding  $e_t$  preserves  $\text{Dispersion}(C \cup \{e_t\}) < \rho$ .

If both constraints are satisfied,  $e_t$  is added to the current cluster. If either is violated, a *violation counter* is incremented. When the violation counter exceeds  $\kappa$ , the cluster is closed and its center of gravity is computed. An iteration  $t$  is classified as an *outlier* if it occurs during an active cluster and violates at least one constraint, but consecutive violations have not yet exceeded the patience

threshold  $\kappa$ . Outliers are excluded from the cluster’s center of gravity computation, but the cluster remains open until more than  $\kappa$  consecutive violations occur.

This incremental procedure detects multiple clusters along a trajectory, each characterized by its center of gravity (attractor), temporal extent and semantic dispersion.

## 6.7 Cluster Trajectory Visualization

To visualize cluster membership and semantic stability along an agentic trajectory, we construct a two-dimensional representation that encodes cluster identity, attractor similarity and outlier status simultaneously.

**Graph construction.** For a trajectory with  $m$  detected clusters  $\{C_1, \dots, C_m\}$ , each cluster  $C_i$  is assigned a baseline at  $y = i$ . For each iteration  $t$  belonging to cluster  $C_i$  (i.e.,  $t \in [t_a^i, t_b^i]$ ), we plot a point at coordinates:

$$(x, y) = (t, i + \alpha \cdot d(t, C_i)), \quad \text{where} \quad d(t, C_i) = 1 - \tilde{s}(e_t, a_i). \quad (23)$$

Here,  $a_i$  is the attractor of cluster  $C_i$  and  $\tilde{s}$  is the calibrated similarity. The vertical offset  $d(t, C_i)$  measures how far embedding  $e_t$  deviates from the cluster’s attractor in similarity space. A scaling factor  $\alpha > 0$  amplifies vertical displacements for better visualization of small deviations.

Points are colored by membership status:

- **Blue points:** valid cluster members ( $t \in [t_a^i, t_b^i] \setminus O_i$ ), contributing to attractor computation
- **Red points:** outliers ( $t \in O_i$ ), excluded from attractor but within patience threshold  $\kappa$

A grey band of height  $\alpha \cdot \rho$  around each baseline  $y = i$  visualizes the dispersion constraint: all blue points must remain below  $y = i + \alpha \cdot \rho$  for the cluster to satisfy the dispersion constraint.

**Reading the graph.** The vertical position encodes semantic proximity to the attractor:

- A point at  $y = i$  indicates  $\tilde{s}(e_t, a_i) = 1$  (embedding identical to attractor)
- A point at  $y = i + \alpha \cdot 0.1$  indicates  $\tilde{s}(e_t, a_i) = 0.9$  (high similarity)
- Maximum vertical spread of blue points equals  $\alpha \cdot \text{Dispersion}(C_i)$

Tight clusters exhibit blue points clustered near the baseline, while dispersed clusters show wider vertical spread. Red outliers reveal iterations where the patience mechanism allows temporary violations without terminating the cluster. Gaps between clusters indicate transition periods where the trajectory does not belong to any detected cluster.

## 7 Experimental Study of Singular Agentic Loops

Having established the theoretical framework for analyzing agentic loop dynamics, we now turn to empirical validation. As discussed in Section 6.2, singular loops represent the simplest agentic structure: a single transformation  $F$  applied recursively. By studying singular loops first, we can isolate fundamental dynamical phenomena (contraction, exploration, attractor formation) without the additional complexity introduced by multi-step compositions. This foundational understanding is essential: composite loops, which alternate between generative and critical phases and graph based loops, which coordinate multiple interacting agents, both build upon the basic dynamics characterized here. The experiments presented in this section demonstrate that even the simplest agentic loops exhibit rich, regime-dependent behavior, validating the geometric framework and establishing empirical benchmarks for future studies of more complex architectures.

### 7.1 Experimental Design

To empirically characterize the dynamics of agentic loops, we conduct a controlled experiment using two minimal *singular* loops executed under identical computational conditions. Both operate in the artifact space  $\mathcal{A}$  as purely textual transformations applied iteratively through a single LLM

call per step. The objective is to observe whether distinct prompt formulations can induce fundamentally different dynamic regimes, specifically one exhibiting *contractive* behavior and another exhibiting *exploratory* divergence.

**LLM configuration.** All experiments are performed locally using the O1lama inference framework (version 0.12.9) with the `deepseek-r1:8b` model. This model provides a lightweight yet expressive transformer architecture, suitable for studying fine-grained textual transformations over multiple recursive steps. We use a sampling temperature of 0.8, which introduces mild stochasticity while preserving semantic coherence, ensuring that the observed trajectories reflect both the model’s internal tendencies and the intrinsic stability of the prompt formulation. No explicit random seed was specified, so each generation uses one determined by the inference framework, contributing to the stochastic nature of the observed dynamics.

**Motivation.** The purpose of this experiment is not to model complex reasoning or task-solving behavior, but rather to reveal that even the simplest iterative linguistic transformations can produce structured dynamics when observed in the calibrated semantic space  $(\mathcal{E}, \tilde{s})$ . By isolating the loop mechanism to a single prompt applied recursively, we eliminate confounding factors such as multi-step planning or external memory accumulation. This enables direct observation of the intrinsic dynamical tendencies of the language model itself.

**Experimental setup.** Each loop is defined by a fixed prompt template  $P$ , into which the current artifact  $a_t$  is inserted at each iteration:

$$a_{t+1} = F(a_t) = \text{LLM}(P(a_t)). \quad (24)$$

The process is repeated for  $T = 50$  iterations, generating a trajectory  $\{a_t\}_{t=0}^T$  and its projection  $\{e_t = \psi(a_t)\}_{t=0}^T$  in the representation space  $\mathcal{E}$ . All trajectories are embedded using the same function  $\psi$  and analyzed in the calibrated similarity space defined in Section 4.

**Initial condition.** Both loops are initialized with the same starting sentence:

"Music has the power to connect people across cultures and generations."

This neutral, semantically coherent sentence serves as the common baseline  $a_0$  for comparing the contractive and exploratory dynamics.

**Cluster detection configurations.** To identify emergent structures such as clusters or attractors within each trajectory, we apply the incremental cluster detection algorithm described in Section 6.6. We explore multiple parameter configurations  $(\lambda, \rho, \kappa)$  to assess the robustness of attractor detection under varying spatial resolutions:

$$(\lambda, \rho, \kappa) \in \{(0.8, 0.1, 2), (0.8, 0.2, 2), (0.8, 0.3, 2)\}. \quad (25)$$

This grid allows both fine-grained and coarse-grained analyses of the clustering structure, ensuring that attractor detection is not an artifact of a single threshold choice.

**Prompts and expected regimes.** We define two archetypal prompts designed to induce contrasting dynamical behaviors in the same linguistic space.

- **Contractive loop prompt:**

You are a rewriting agent. At each step, rewrite the sentence to make it sound slightly more natural and fluent, while preserving the meaning exactly.  
 Current sentence: `{{TEXT}}`  
 Provide only the new sentence.

This formulation encourages small, directionally consistent improvements toward a stable expression, leading to decreasing semantic displacement over time. We hypothesize that its trajectory in  $\mathcal{E}$  will converge toward a unique attractor, a locally optimal point corresponding to the most fluent paraphrase of the initial sentence.

- **Exploratory loop prompt:**

Summarize the current text in one sentence, then negate its main idea completely in an abstract way.  
 Current sentence: `{{TEXT}}`  
 Provide only the new sentence.

In contrast, this prompt enforces semantic inversion at each step, deliberately perturbing the meaning while maintaining grammatical coherence. The expected effect is a divergent or oscillatory trajectory in  $\mathcal{E}$ , where successive iterations alternate between semantically distant regions without stabilization.

**Analysis objectives.** To characterize the emergent dynamics, we analyze each trajectory  $\{e_t\}$  according to the following criteria:

1. The sequence of *pairwise displacements*  $\|e_t - e_{t-1}\|_2$  and calibrated similarities  $\tilde{s}(e_t, e_{t-1})$ , quantifying instantaneous dynamics.
2. The evolution of the distance  $\|e_t - e_0\|_2$  and similarity  $\tilde{s}(e_t, e_0)$  to the initial state, capturing long-term semantic drift or contraction.
3. The detection and temporal persistence of *clusters* and *attractors* as defined in Section 6.2, revealing whether the loop settles into recurrent stable regions or exhibits perpetual divergence.

A contractive loop is expected to produce a single dense cluster of high internal similarity, corresponding to a stable attractor. Conversely, an exploratory loop should either fail to produce persistent clusters or exhibit transient, disjoint attractors, reflecting alternating semantic polarity and non-convergent trajectories. These contrasting behaviors form the empirical foundation for the study of dynamics and stability in subsequent analyses.

## 7.2 Contractive Loop Dynamics

This subsection presents the empirical results obtained from the contractive loop. For each configuration of the clustering parameters  $(\lambda, \rho, \kappa)$ , we analyze the resulting trajectory in the calibrated embedding space  $(\mathcal{E}, \tilde{s})$ , focusing on the emergence of clusters, attractors and inter-cluster similarity patterns.

The contractive loop was designed to iteratively refine a sentence while preserving its semantic meaning. As expected, the observed trajectory rapidly converges toward a small, dense region in  $\mathcal{E}$ , revealing a clear attractor structure. We first analyze the overall geometric behavior of the trajectory, independent of any clustering configuration, before examining how different density thresholds  $(\lambda, \rho, \kappa)$  reveal the underlying attractor organization. The complete sequence of generated artifacts is provided in Appendix A for reference.

### 7.2.1 Global and Local Dynamics

Figure 9 presents the evolution of both local and global geometric metrics along the trajectory of 50 iterations. These indicators provide a direct view of the loop’s dynamics before any segmentation into clusters.

**Local stability.** The local Euclidean distance  $\|e_t - e_{t-1}\|_2$  fluctuates between 0.45 and 0.55, while the corresponding calibrated similarity  $\tilde{s}(e_t, e_{t-1})$  remains consistently high in the range 0.82–0.95. This indicates that each rewriting step introduces only minimal changes to the representation, consistent with the model’s smooth behavior under incremental rewriting.

**Global convergence.** When compared to the initial state  $e_0$ , the global distance stabilizes around 0.6 and the calibrated similarity remains near 0.75. After a few initial iterations, the trajectory stops drifting and remains confined within a bounded region of  $\mathcal{E}$ , consistent with the expected contractive regime. This global stability validates the use of local geometric measures as reliable indicators of semantic convergence.

**Interpretation.** The consistency between local and global patterns shows that the operator  $F$  exhibits local contractivity in practice, despite no formal guarantee on  $\psi$ ’s continuity. The contractive loop thus defines a smooth trajectory approaching an equilibrium region, setting the stage for

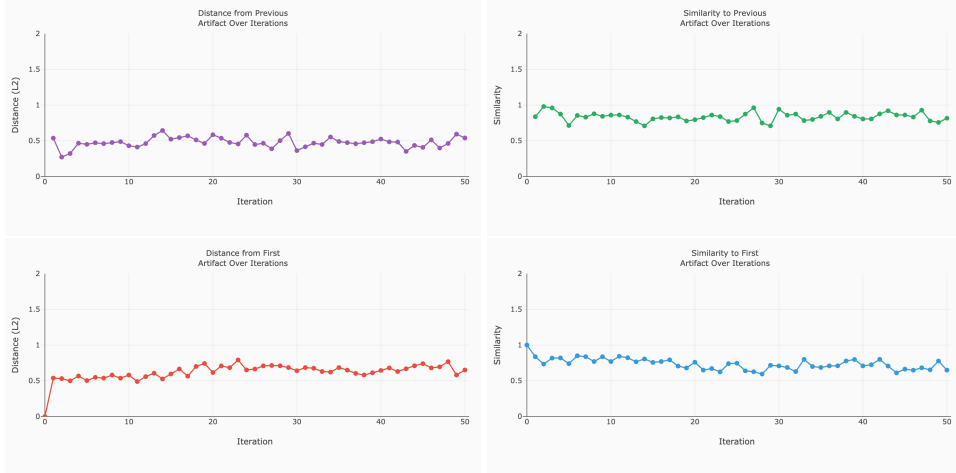


Figure 9: Local and global geometric evolution of the contractive loop trajectory. (Top) Local distances and similarities between consecutive embeddings ( $e_t, e_{t-1}$ ). (Bottom) Global distances and similarities relative to the initial embedding  $e_0$ .

a finer-grained analysis of its attractor structure through clustering. These observations are consistent with  $\mathcal{R}_{\text{ctr}}$  as formally defined in Section 6.5: the trajectory exhibits behavior consistent with convergence toward a stable region in  $\mathcal{E}$ , approximating a fixed point attractor.

### 7.2.2 Cluster and Attractor Analysis

We now apply the density-based clustering framework defined in Section 6.2 to characterize how the trajectory organizes into stable subregions or attractors. Three clustering configurations were tested, varying only the spatial radius  $\rho$  while keeping  $\lambda = 0.8$  and  $\kappa = 2$  constant.

**Configuration**  $(\lambda, \rho, \kappa) = (0.8, 0.1, 2)$ . This most restrictive configuration identifies only tightly packed regions in the embedding space. Five clusters were detected, corresponding to distinct stabilization phases during the trajectory.

Cluster	Iteration Range	Dispersion	Outliers
Cluster 1	0–3	0.0648	2
Cluster 2	6–12	0.0400	2
Cluster 3	15–17	0.0400	2
Cluster 4	20–27	0.0967	4
Cluster 5	30–47	0.0800	8

Table 4: Cluster configuration for the contractive loop under  $(\lambda, \rho, \kappa) = (0.8, 0.1, 2)$ .

Figure 10 shows the temporal progression of cluster memberships. The transition between clusters follows a smooth temporal sequence rather than abrupt shifts, reflecting progressive refinement.

**Attractor similarity matrix.** The inter-cluster similarity matrix (Table 5) reveals strong geometric coherence among all cluster centroids.

All off-diagonal similarities remain above 0.78, consistent with the observation that even when the trajectory transiently visits different micro-regions, these remain tightly aligned in the semantic manifold. Clusters 4 and 5 exhibit the highest cohesion and persistence, suggesting convergence toward a single dominant attractor.

**Interpretation.** The contractive loop thus exhibits a robust convergence regime characterized by:

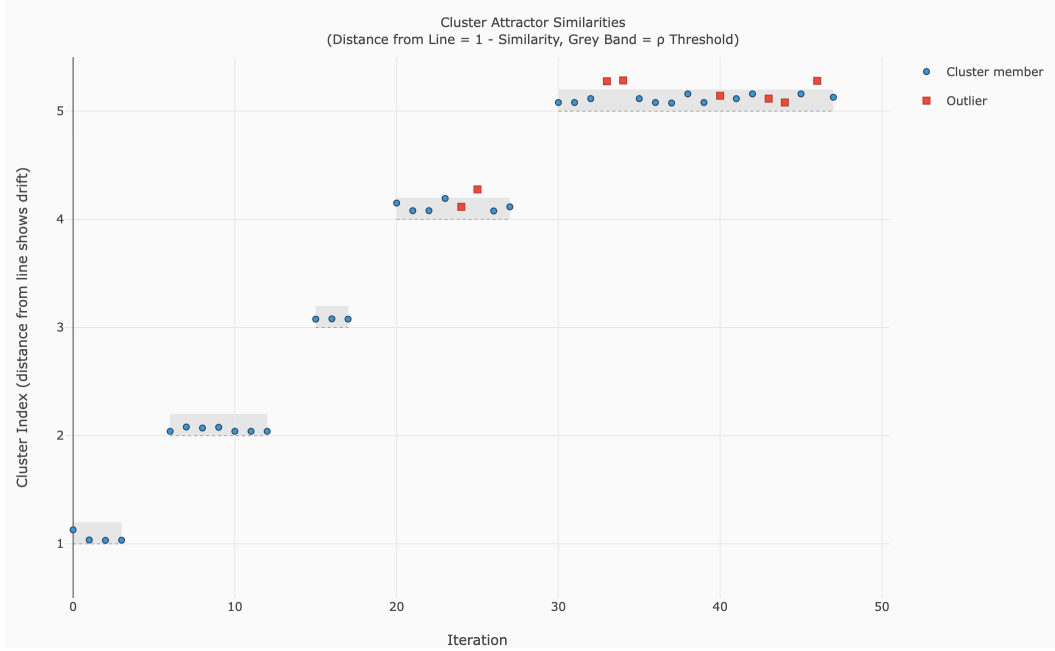


Figure 10: Cluster membership timeline for the contractive loop under  $(\lambda, \rho, \kappa) = (0.8, 0.1, 2)$ . Outliers are marked in red. The sequence shows smooth temporal progression through five stabilization phases.

	<b>C1</b>	<b>C2</b>	<b>C3</b>	<b>C4</b>	<b>C5</b>
<b>C1</b>	1.0000	0.9800	0.8060	0.8580	0.8500
<b>C2</b>	0.9800	1.0000	0.8326	0.7956	0.7804
<b>C3</b>	0.8060	0.8326	1.0000	0.7937	0.8600
<b>C4</b>	0.8580	0.7956	0.7937	1.0000	0.9800
<b>C5</b>	0.8500	0.7804	0.8600	0.9800	1.0000

Table 5: Attractor Similarity Matrix for the contractive loop  $(\lambda, \rho, \kappa) = (0.8, 0.1, 2)$ .

- bounded local and global geometric variation;
- smooth temporal progression across increasingly stable clusters;
- and a high-density attractor region exhibiting inter-cluster similarity above 0.8.

From a linguistic perspective, this behavior reflects progressive syntactic smoothing and stylistic normalization: the LLM converges toward a canonical phrasing that represents an equilibrium point in the semantic manifold.

**Configuration**  $(\lambda, \rho, \kappa) = (0.8, 0.2, 2)$ . When the clustering radius is increased to  $\rho = 0.2$ , smaller micro-clusters merge into broader regions, revealing a simplified attractor landscape composed of only two persistent clusters. These clusters correspond to two major stabilization phases within the contractive trajectory: an initial transient phase and a final convergence basin.

<b>Cluster</b>	<b>Iteration Range</b>	<b>Dispersion</b>	<b>Outliers</b>
Cluster 1	0–18	0.1773	6
Cluster 2	21–50	0.1500	9

Table 6: Cluster configuration for the contractive loop under  $(\lambda, \rho, \kappa) = (0.8, 0.2, 2)$ .

The temporal organization of the trajectory, shown in Figure 11, confirms a single transition between two stable basins. The early iterations (Cluster 1) exhibit slightly higher dispersion, while the second phase (Cluster 2) displays long persistence and near-perfect internal similarity.

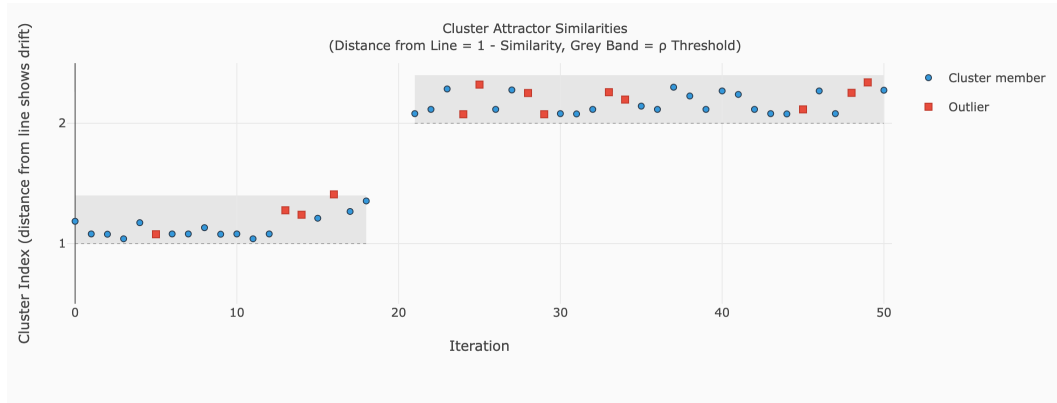


Figure 11: Cluster membership timeline for the contractive loop under  $(\lambda, \rho, \kappa) = (0.8, 0.2, 2)$ . Each point represents an iteration, color-coded by cluster membership. Outliers (in red) correspond to transient points at cluster boundaries.

**Attractor similarity matrix.** The inter-cluster similarity matrix in Table 7 shows that both clusters are strongly aligned in the embedding space, with a centroid similarity of 0.89.

	C1	C2
C1	1.0000	0.8900
C2	0.8900	1.0000

Table 7: Attractor Similarity Matrix for the contractive loop  $(\lambda, \rho, \kappa) = (0.8, 0.2, 2)$ .

The high centroid similarity confirms that the two attractors occupy closely neighboring regions in  $\mathcal{E}$ , consistent with a smooth convergence process. The transition between them occurs around iteration 20 and marks the point where the rewriting process reaches its asymptotic stability.

**Interpretation.** Compared to the previous configuration ( $\rho = 0.1$ ), this setting highlights the macro-scale structure of the trajectory: the loop first explores a transient manifold (Cluster 1) before collapsing into a single dense attractor (Cluster 2). The overall trajectory thus reflects a monotonic contraction process toward a stable equilibrium region, with no evidence of oscillation or divergence.

**Configuration**  $(\lambda, \rho, \kappa) = (0.8, 0.3, 2)$ . At a larger radius  $\rho = 0.3$ , the clustering process identifies a single dense region encompassing the entire trajectory. This configuration effectively merges all transient substructures into one unified attractor, consistent with the strongly contractive nature of the rewriting loop.

Cluster	Iteration Range	Dispersion	Outliers
Cluster 1	0–50	0.2100	13

Table 8: Cluster configuration for the contractive loop under  $(\lambda, \rho, \kappa) = (0.8, 0.3, 2)$ .

The corresponding temporal distribution, shown in Figure 12, confirms the absence of any segmentation: all iterations are assigned to the same cluster, with a few boundary outliers reflecting minimal fluctuations near the threshold  $\rho = 0.3$ .

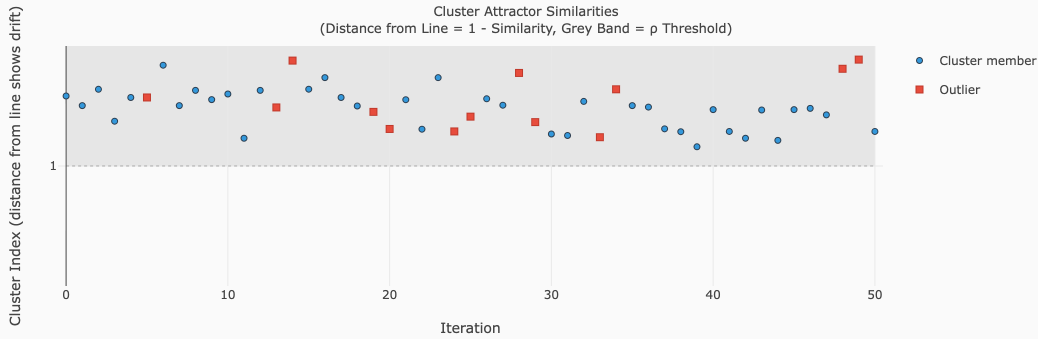


Figure 12: Cluster membership timeline for the contractive loop under  $(\lambda, \rho, \kappa) = (0.8, 0.3, 2)$ . All iterations belong to a single dense cluster, with minor outliers (in red) near the stability boundary.

**Interpretation.** The detection of a single persistent cluster across all iterations confirms that the rewriting operator  $F$  acts as a strong contraction mapping in  $(\mathcal{E}, \tilde{s})$ . Even under relaxed density constraints, no internal bifurcation or oscillatory pattern emerges. This configuration thus captures the fixed-point regime of the loop, where the generated sentences become semantically and stylistically indistinguishable over time.

**Summary of clustering outcomes.** When the clustering radius  $\rho$  increases to 0.2 or above, micro-clusters merge into a single dense region, effectively collapsing the entire trajectory into one stable attractor. This collapse into a single dense attractor empirically validates the  $\mathcal{R}_{\text{ctr}}$  definition (Section 6.5), suggesting convergence toward a stable fixed point in the embedding space. No secondary structure is detected for  $\rho \geq 0.2$ , consistent with a globally contractive process with negligible oscillation. However, these observations are based on  $T = 50$  iterations. While the trajectory shows no signs of leaving the attractor within this window, we cannot formally guarantee that oscillations or cluster exits would not occur over longer horizons. The empirical stability observed here suggests such escapes are unlikely, but proving this rigorously would require a more advanced mathematical framework, for instance analyzing the probability of entering and remaining within a cluster as a function of the transformation operator  $F$  and the embedding geometry.

### 7.3 Exploratory Loop Dynamics

In contrast to the previous rewriting loop, the exploratory loop was designed to alternate between summarization and semantic negation. This alternation introduces an intrinsic instability in the semantic space, continuously disrupting coherence and preventing any convergence toward a stable region of  $\mathcal{E}$ . The resulting trajectory exhibits high variability and recurrent semantic inversions, typical of a divergent or oscillatory dynamic. The complete sequence of generated artifacts is provided in Appendix B for reference.

#### 7.3.1 Global and Local Dynamics

Figure 13 presents the evolution of both local and global geometric metrics over 50 iterations. Unlike the contractive regime, these indicators show strong irregularity and the absence of any stabilization phase.

**Local instability.** The local Euclidean distance  $\|e_t - e_{t-1}\|_2$  remains high across iterations, oscillating between 0.8 and 1.3 with no decreasing trend. Similarly, the local similarity  $\tilde{s}(e_t, e_{t-1})$  fluctuates widely between 0.2 and 0.6, occasionally dropping close to zero. These erratic variations indicate that each step produces a major semantic reorientation rather than a refinement of the previous state.

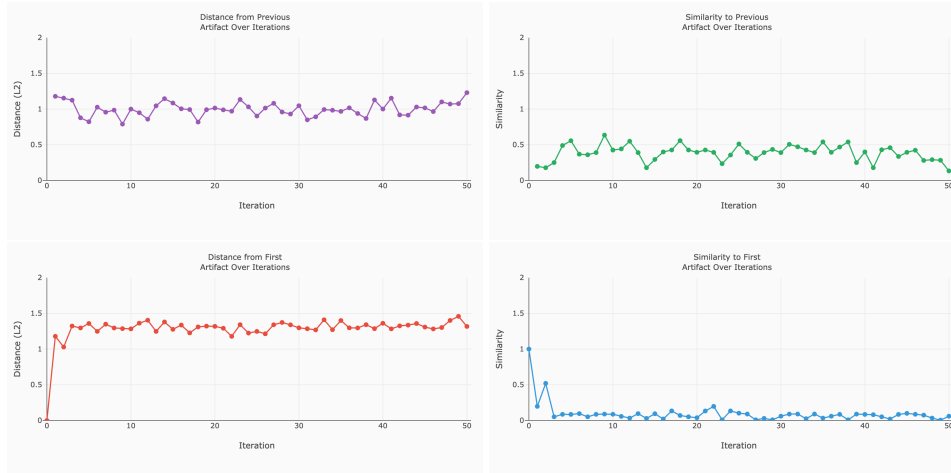


Figure 13: Local and global geometric evolution of the exploratory loop trajectory. (Top) Local distances and similarities between consecutive embeddings  $(e_t, e_{t-1})$ . (Bottom) Global distances and similarities relative to the initial embedding  $e_0$ .

**Global divergence.** The global distance to the initial embedding  $e_0$  rapidly increases during the first iterations and stabilizes around  $\|e_t - e_0\|_2 \approx 1.3$  (see Figure 13, bottom left). The corresponding global similarity  $\tilde{s}(e_t, e_0)$  remains very low (mostly below 0.2), consistent with a loop that continuously generates artifacts semantically unrelated to the starting point. This behavior reveals the absence of any long-term memory or attractor basin in the semantic manifold.

**Interpretation.** The exploratory loop behaves as a *divergent operator* in  $(\mathcal{E}, \tilde{s})$ . Each iteration projects the embedding into a distant and nearly orthogonal region of the space, breaking any potential contractive pattern. The trajectory thus explores disconnected semantic areas rather than converging toward an equilibrium. This persistent divergence and absence of convergence align with  $\mathcal{R}_{\text{exp}}$  as formally defined in Section 6.5: unbounded or aperiodic movement within  $\mathcal{E}$  with no stable attractor. As with the contractive case, these observations are limited to  $T = 50$  iterations. We cannot formally exclude the possibility that a cluster might eventually form over longer horizons. However, the consistently high inter-iteration distances suggest this is unlikely. A rigorous characterization would require a mathematical framework for analyzing the probability of cluster formation under a given transformation operator.

### 7.3.2 Clustering Attempt and Absence of Attractors

To test whether transient structures could still emerge locally, we applied the same density-based clustering procedure as for the contractive loop. However, no valid cluster was detected under any tested configuration. This complete absence of clusters directly confirms  $\mathcal{R}_{\text{exp}}$  behavior (Section 6.5): the trajectory exhibits no stable attractor basin.

This failure to identify clusters reflects the fundamental instability of the exploratory process: the embeddings never remain within a stable neighborhood long enough to satisfy the density or similarity conditions required for cluster formation.

**Empirical evidence.** Throughout the 50 iterations, each embedding violates the spatial proximity criterion  $\rho$  almost immediately after creation. The lack of recurrence, combined with high inter-step distances and very low similarities, results in a completely dispersed point cloud in  $\mathcal{E}$ .

**Geometric interpretation.** The absence of attractors implies that the transformation function  $F$  induced by this loop does not define a bounded trajectory. Instead,  $F$  exhibits a form of *semantic exploration*: each output resets the contextual reference frame, pushing the system toward a new region of the manifold that bears little relation to the previous one.

**Summary.** The exploratory loop displays:

- persistent high local distances ( $\|e_t - e_{t-1}\|_2 \approx 1.0$ ) and low similarities ( $\bar{s} < 0.5$ );
- no geometric stabilization, either locally or globally;
- and the complete absence of clusters or attractor basins for all tested parameters.

In semantic terms, this loop corresponds to a continuous destruction and regeneration of meaning: each iteration rewrites the narrative space from scratch, producing an intrinsically non-convergent agentic dynamic.

### 7.4 Comparative Summary

The empirical analysis of contractive and exploratory loops reveals fundamentally distinct dynamical regimes, following the formal definitions established in Section 6.5. Table 9 summarizes the key quantitative and qualitative differences between these two archetypal behaviors.

Metric	Contractive Loop	Exploratory Loop
Mean local distance	$\sim 0.5$	$\sim 1.0$
Mean local similarity	$> 0.85$	$< 0.5$
Clusters detected	$5 \rightarrow 1$	0
Global drift	Bounded	Unbounded
Regime type	Convergent	Divergent

Table 9: Comparative summary of contractive and exploratory agentic loop dynamics.

These results provide empirical evidence for the existence of distinct dynamic regimes in recursive generative systems. The contractive loop exhibits progressive semantic refinement, converging toward a stable attractor as evidenced by high local similarity ( $> 0.85$ ) and bounded global drift. In contrast, the exploratory loop exhibits persistent instability, with each iteration producing semantically distant outputs ( $\sim 1.0$  Euclidean distance) and no detectable cluster structure. This dichotomy confirms that the choice of prompt and transformation operator fundamentally determines the long-term behavior of agentic trajectories, ranging from stable convergence to unbounded semantic wandering.

## 8 Discussion and Perspectives

The empirical results presented above highlight two extreme regimes of agentic dynamics within the embedding manifold  $(\mathcal{E}, \bar{s})$ :  $\mathcal{R}_{ctr}$ , characterized by convergence toward a stable attractor, and  $\mathcal{R}_{exp}$ , marked by unbounded divergence and the absence of any stable region. These two archetypal behaviors constitute the endpoints of a broader spectrum of agentic dynamics that could potentially be modulated, combined or even harnessed for creative control.

### 8.1 Model Dependence and Generalization

A first natural extension concerns the robustness of these observations across different embedding models and language models.

**Embedding representations.** The current study relies on a single embedding function  $\psi$  to project textual artifacts into  $\mathcal{E}$ . However, various embedding architectures exhibit distinct geometric anisotropies and similarity landscapes. Future work should therefore replicate the same agentic trajectories across multiple embedding backbones to evaluate whether contraction and exploration are intrinsic to the generative process  $F$  or contingent upon the metric structure of  $\mathcal{E}$ .

**Language models.** Similarly, the generation operator  $F$  depends on the underlying LLM and its internal sampling mechanisms. Different architectures (e.g., GPT, Claude, Mistral, Llama) and decoding settings (temperature, top- $p$ , beam search) may alter dynamics of  $F$ . A comparative study could determine whether exploratory dynamics arise from semantic inversion per se or from model-specific sampling noise.

## 8.2 Toward Composite Agentic Loops

Beyond the study of isolated transformations, a promising avenue is the investigation of *composite loops*, where contractive and exploratory iterations alternate within a single process. Such compositions could emulate a controlled exploration–consolidation cycle:

$$F_{\text{composite}} = F_{\text{contractive}} \circ F_{\text{exploratory}} \quad \text{or} \quad F_{\text{exploratory}} \circ F_{\text{contractive}}. \quad (26)$$

Intuitively, an exploratory iteration could inject novelty and creative divergence, while a subsequent contractive step would restore semantic coherence and bring the system back toward a stable region. This dual-phase regime might enable the construction of agents that balance *creative drift* and *semantic control*, producing bounded yet innovative trajectories within  $\mathcal{E}$ .

The quantitative analysis of such mixed loops would require monitoring:

- the alternation between expansion (entropy increase) and contraction (entropy reduction);
- the long-term recurrence or periodicity of the resulting trajectory;
- and the net displacement relative to the initial semantic manifold.

## 8.3 Toward Geometry of Agentic Cognition

The trajectory analysis framework developed in this paper enables a natural question: can an agentic loop *reason about its own geometric dynamics* and adapt its behavior to achieve specific objectives? This motivates a future research direction we term **Geometry of Agentic Cognition**: systems where the agent possesses geometric self-awareness and can metacognitively control its trajectory evolution.

**Current state: external control.** Presently, trajectory control remains external to the loop itself. The intensity of contraction or exploration can be modulated through:

- **Prompt engineering:** adjusting the degree of rewriting, abstraction or negation in the instruction layer;
- **Sampling parameters:** manipulating temperature, nucleus probability (top-p), top-k or repetition penalties to alter stochasticity.

These mechanisms require external intervention: a human engineer or outer control system must specify parameters a priori.

**Future direction: agentic geometric cognition.** A fundamentally different paradigm would enable the agentic loop itself to *observe, reason about and adapt* its trajectory dynamics based on geometric awareness. In this vision, at each iteration  $t$ , the agent would:

1. **Observe trajectory geometry:** Compute calibrated similarities  $\tilde{s}(e_t, e_{t-1})$  (local dynamics),  $\tilde{s}(e_t, e_0)$  (global drift) and trajectory dispersion to assess its current dynamical regime.
2. **Reason about objective alignment:** Evaluate whether its trajectory is progressing toward the desired objective, whether convergence toward a solution (requires contraction), exploration of alternatives (requires divergence) or escape from a suboptimal attractor (requires controlled instability).
3. **Adapt iteration strategy:** Based on this geometric self-assessment, metacognitively adjust the next transformation by increasing exploration if trapped in local minima, inducing contraction if approaching the target region or maintaining the current regime if progressing optimally.

This would transform agentic loops from passive trajectory executors into *geometric navigators*: systems that understand their position in semantic space and actively steer toward objectives through informed dynamical control.

**Enabling mechanisms.** Implementing agentic geometric cognition requires:

- **Trajectory introspection:** Embedding the agent’s own outputs  $\{a_0, a_1, \dots, a_t\}$  and computing geometric indicators (similarity, dispersion, clustering metrics) as part of the loop context.
- **Geometric prompt characterization:** Pre-characterizing prompts by their dynamical properties (contractive, exploratory) and selecting from a prompt library based on desired trajectory behavior. This requires a mathematical framework capable of predicting a prompt’s dynamical regime *a priori*, which we address in forthcoming work.
- **Adaptive parameter control:** Allowing the agent to specify its own generation parameters or select from predefined strategies (e.g., "use high-temperature exploration" vs. "use low-temperature refinement") based on trajectory analysis.

This research direction opens fundamental questions at the intersection of dynamical systems, metacognition and autonomous reasoning: Can language models learn to recognize geometric patterns in their own trajectories? Can they develop heuristics for when to contract versus explore based on objective alignment? Can they generalize trajectory control strategies across different tasks? The geometric framework established in this paper provides the measurement infrastructure required to empirically investigate these questions, enabling rigorous quantification of whether and how agentic systems can achieve geometric self-regulation.

#### 8.4 Application: Creativity as Objective

The agentic geometric cognition framework introduced in Section 8.3 raises a natural application question: what if the *objective* that the agent targets is to *maximize creativity*? This section explores how computational creativity, formalized by Boden [1] as exploration-transformation-combination processes and by Colton and Wiggins [2] as novelty-value-surprise dimensions, can be operationalized as a specific objective within the geometry of agentic cognition framework.

**Creativity metrics as geometric observables.** To target creativity as an objective, an agent with geometric self-awareness must first be able to *measure* creativity dimensions along its trajectory. Our geometric framework provides measurable indicators that correspond to Colton & Wiggins’ creativity dimensions:

- **Novelty** corresponds to exploratory dynamics, that is, trajectories that visit diverse regions of semantic space without settling into stable attractors. The absence of persistent clusters and low calibrated similarity between consecutive states ( $\bar{s}(e_t, e_{t-1})$ ) indicate ongoing exploration that generates new ideas rather than refining existing ones.
- **Value** corresponds to convergence toward stable attractors with low dispersion. Trajectories that stabilize around a fixed point produce semantically coherent, trustworthy outputs. Conversely, divergent trajectories exhibit semantic drift, where outputs lose coherence and become unreliable, yielding low value.
- **Surprise** corresponds to sudden, unpredictable semantic transitions, specifically trajectory discontinuities where the semantic state jumps sharply after periods of stability. Contractive loops exhibit low surprise (smooth, predictable convergence), while exploratory loops may produce high surprise through unpredictable jumps between distant semantic regions.

This operationalization enables *measurable creativity control*. Boden’s exploratory creativity can be triggered within agentic loop iterations by introducing high-temperature sampling and role-based divergent prompts [3] (for instance, adopting perspectives such as an artist, a child or a poet), which induce high dispersion and novelty generation. However, unconstrained exploration risks semantic drift and loss of value. To balance creativity, subsequent iterations can act as *consolidators*, employing role-based contractive prompts (e.g., scientist, engineer, critic) that reduce dispersion and restore coherence, maximizing value while preserving novel content.

**Composite loops as creativity engines.** This dual-phase architecture naturally maps to *composite loops* as defined in Section 6.2. A composite loop with two phases per iteration would take the form:

$$a_{t+1} = \text{LLM}_{\text{contract}}(P_{\text{contract}}(\text{LLM}_{\text{explore}}(P_{\text{explore}}(a_t)))), \quad (27)$$

where  $P_{\text{explore}}$  uses role-based divergent prompts (e.g., "adopt the perspective of an artist") to induce exploratory divergence and  $P_{\text{contract}}$  employs precision-oriented prompts (e.g., "critically evaluate and consolidate") to enforce contraction. The generation parameters can be tuned accordingly:  $\text{LLM}_{\text{explore}}$  could use high temperature (e.g.,  $T = 1.2$ ) for creative diversity, while  $\text{LLM}_{\text{contract}}$  could use low temperature (e.g.,  $T = 0.3$ ) for deterministic refinement. The singular loop experiments presented in Section 7 establish that these individual  $(P, \text{LLM})$  pairs can reliably induce their respective regimes. Composing them sequentially would create an oscillatory dynamic where each iteration explores the semantic manifold then contracts toward coherent outputs, effectively implementing Boden’s explore-transform-combine cycle through geometric dynamics.

The interplay between these regimes may enable a new kind of *controlled computational creativity*, where the balance between exploration and consolidation is explicitly managed through prompt design, role assignment and iterative feedback. Future work could formalize this balance through composite loop architectures that adaptively modulate their dynamics based on creativity objectives, bridging Boden’s theoretical framework with the geometric formalism introduced here.

## 8.5 Extending Toward Complex Agentic Architectures

Finally, the framework introduced here can be generalized beyond singular loops to more complex agentic architectures composed of interacting subloops, each operating under distinct dynamics and objectives. Examples include:

- hierarchical loops, where upper layers modulate the contractive or exploratory tendency of lower layers;
- cooperative loops, in which multiple agents operate in parallel within shared embedding subspaces;
- and adversarial or self-reflective loops, where one agent destabilizes while another re-stabilizes the shared representation.

Such architectures could reveal emergent phenomena such as collective attractors, dynamic equilibrium points or oscillatory creative states, bridging the gap between low-level generative processes and higher-order cognitive modeling.

**Outlook and Future Directions.** By formalizing agentic dynamics in terms of their geometric behavior within embedding spaces, this work opens the path to a quantitative study of creativity and stability in language models. Future research on composite, parameterized and hierarchical agentic loops may ultimately lead to the design of *controllable creative agents*: systems capable of exploring without drifting and stabilizing without stagnating. This discussion opens the way to broader formal and experimental investigations, which are summarized in the final conclusion.

## 9 Conclusion

This work introduced a geometric framework for analyzing the dynamics of agentic loops: recursive processes in which large language models iteratively transform their own outputs. By grounding these dynamics in a calibrated semantic embedding space  $(\mathcal{E}, \tilde{s})$  that enables human-aligned measurements, we made it possible to quantify how iterative LLM processes unfold, stabilize or diverge across iterations.

**Summary of contributions.** The study provides three main contributions:

1. A formal distinction between the *artifact space*  $(\mathcal{A}, F)$ , where linguistic transformations occur, and its continuous *representation space*  $(\mathcal{E}, \|\cdot\|)$ , enabling quantitative measurement of agentic dynamics through geometric trajectory analysis.
2. A calibrated similarity metric  $\tilde{s} = f_{\text{isotonic}} \circ s^{(m)}$  that corrects the anisotropy of embedding spaces and provides human-aligned geometric indicators: dispersion, displacement, cluster coherence and trajectory discontinuities.
3. An empirical demonstration that agentic loops exhibit distinct dynamical regimes (contractive or exploratory) depending solely on their prompt formulation, with measurable geometric signatures that characterize each regime.

**Empirical findings.** Using a controlled experimental setup, we showed that:

- The **contractive loop**, driven by incremental rewriting, produces a smooth and bounded trajectory in  $\mathcal{E}$  that converges toward a dense attractor region. Its dynamics exhibit local contractivity: successive embeddings remain close, dispersion decreases over time, and the trajectory stabilizes within persistent clusters.
- The **exploratory loop**, built on alternating summarization and negation, generates an unbounded trajectory with no persistent clusters or attractors. Its behavior is characterized by high local displacements and low inter-iteration similarity, with dispersion remaining elevated throughout the process.

Together, these two regimes define a spectrum of agentic dynamics, from convergent stabilization to divergent exploration, each with distinct geometric signatures.

**Theoretical implications.** From a dynamical systems perspective, these observations are consistent with a view of LLM-based transformations  $F$  as mappings whose dynamics resemble those governed by an effective contraction rate:

$$\|F(a_1) - F(a_2)\| \leq L \|a_1 - a_2\|, \quad L < 1 \Rightarrow \text{contraction}, \quad L > 1 \Rightarrow \text{divergence}. \quad (28)$$

Since  $F$  operates in  $\mathcal{A}$  but all geometric measurements occur in  $\mathcal{E}$  through  $\psi$ , the contraction rate is understood with respect to the induced operator  $\hat{F} = \psi \circ F$ . While such bounds cannot be measured directly for deep generative operators, the observed trajectory patterns suggest a regime-dependent effective contraction rate that could be estimated through embedding-space analysis. This opens the door to a formal theory of *agentic dynamics*, linking prompt design, model sampling and geometric regularity.

**Broader outlook.** The contrast between contractive and exploratory regimes highlights a key tension in autonomous generative systems: the need to balance *semantic exploration* and *stability*. While this paper focused on *singular loops* to establish foundational dynamical phenomena, the natural next step is the study of *composite loops*, structures where multiple LLM calls with different prompts compose sequentially within each iteration:

$$a_{t+1} = \text{LLM}_2(P_2(\text{LLM}_1(P_1(a_t))))). \quad (29)$$

For example, a generate-critique-revise cycle would use  $P_1$  for generation,  $P_2$  for critique and  $P_3$  for revision. The singular loop experiments demonstrated that individual  $(P, \text{LLM})$  pairs can reliably induce contractive or exploratory dynamics. Composing these building blocks offers a systematic path toward *controlled agentic behavior*: alternating exploratory (divergent) and consolidating (contractive) phases to enable agents that explore the semantic space while maintaining coherence.

This principle extends naturally to *complex agentic architectures*, where multiple loops interact, synchronize or self-regulate within shared semantic manifolds. Hierarchical, cooperative and adversarial multi-loop systems could exhibit emergent behaviors (collective attractors, dynamic equilibria or oscillatory states) that go beyond the capabilities of individual loops. Understanding these phenomena requires extending the geometric framework presented here to handle compositions, feedback and synchronization across interacting semantic trajectories.

**Final remark.** Ultimately, this work provides both a language and a methodology for describing the internal geometry of agentic loops in LLMs. By establishing these foundations through singular loop analysis, it opens the path toward understanding composite and complex agentic systems that balance exploration and consolidation. The framework connects naturally to computational creativity research, where the geometric indicators developed here (dispersion, cluster coherence, trajectory discontinuities) can operationalize theoretical notions of novelty, value and surprise. More broadly, it establishes a bridge between agentic AI and dynamical systems theory, encouraging future study of how autonomous generative processes evolve within semantic embedding spaces.

## Acknowledgments

The author thanks open-source contributors of the O11ama and Deepseek projects for enabling reproducible experimentation on local models, the Xenova project for providing a reproducible transformer inference pipeline and the creators of the MTEB STS Benchmark dataset for providing calibrated human similarity judgments.

## Statements and Declarations

### Competing Interests

The author declares that there are no competing financial or non-financial interests that could have influenced the work reported in this paper.

### Data Availability

The experiments were conducted using custom implementations. Code availability will be considered following the peer-review process.

## References

- [1] Margaret A. Boden. Computer models of creativity. *AI Magazine*, 30(3):23–34, 2009.
- [2] Simon Colton and Geraint A. Wiggins. Computational creativity: The final frontier? In *Proceedings of the 20th European Conference on Artificial Intelligence (ECAI 2012)*, pages 21–26. IOS Press, 2012.
- [3] Yunpu Zhao, Rui Zhang, Wenyi Li, Di Huang, Jiaming Guo, Shaohui Peng, Yifan Hao, Yuanbo Wen, Xing Hu, Zidong Du, Qi Guo, Ling Li, and Yunji Chen. Assessing and understanding creativity in large language models. *arXiv preprint arXiv:2401.12491*, 2024.
- [4] Aman Madaan, Niket Tandon, Prakhar Gupta, Skyler Hallinan, Luyu Gao, Sarah Wiegrefe, Uri Alon, Nouha Dziri, Shrimai Prabhunoye, Yiming Yang, et al. Self-refine: Iterative refinement with self-feedback. In *Advances in Neural Information Processing Systems*, volume 36, 2023.
- [5] Jason Wei, Xuezhi Wang, Dale Schuurmans, Maarten Bosma, Brian Ichter, Fei Xia, Ed Chi, Quoc Le, and Denny Zhou. Chain-of-thought prompting elicits reasoning in large language models. In *Advances in Neural Information Processing Systems*, volume 35, pages 24824–24837, 2022.
- [6] Shunyu Yao, Jeffrey Zhao, Dian Yu, Nan Du, Izhak Shafran, Karthik Narasimhan, and Yuan Cao. React: Synergizing reasoning and acting in language models. In *International Conference on Learning Representations*, 2023.
- [7] Noah Shinn, Federico Cassano, Ashwin Gopinath, Karthik Narasimhan, and Shunyu Yao. Reflexion: Language agents with verbal reinforcement learning. In *Advances in Neural Information Processing Systems*, volume 36, 2023.
- [8] Joon Sung Park, Joseph C. O’Brien, Carrie J. Cai, Meredith Ringel Morris, Percy Liang, and Michael S. Bernstein. Generative agents: Interactive simulacra of human behavior. *arXiv preprint arXiv:2304.03442*, 2023.
- [9] Kawin Ethayarajh. How contextual are contextualized word representations? comparing the geometry of bert, elmo, and gpt-2 embeddings. In *Proceedings of the 2019 Conference on Empirical Methods in Natural Language Processing*, pages 55–65, 2019.
- [10] Tongzhou Wang and Phillip Isola. Understanding contrastive representation learning through alignment and uniformity on the hypersphere. In *International Conference on Machine Learning*, pages 9929–9939, 2020.

- [11] Alexandru Niculescu-Mizil and Rich Caruana. Predicting good probabilities with supervised learning. In *Proceedings of the 22nd International Conference on Machine Learning*, pages 625–632, 2005.
- [12] Roman Vershynin. *High-Dimensional Probability: An Introduction with Applications in Data Science*. Cambridge University Press, 2018. Section 5.1.2, Theorem 5.1.3. This result builds on the historical work of Paul Lévy (1951), Milman–Schechtman (1986), and Ledoux (2001) on concentration of measure phenomena.
- [13] Bernard W. Silverman. *Density Estimation for Statistics and Data Analysis*. Chapman and Hall/CRC, London, 1986. Section 3.4 presents the rule of thumb for bandwidth selection.

The appendix provides extended derivations and full experimental sequences for completeness and reproducibility.

## A Contractive Loop: Complete Trajectory

This appendix provides the complete sequence of artifacts generated by the contractive loop experiment described in Section 7. The initial artifact  $a_0$  undergoes 50 iterations of the rewriting transformation, producing the trajectory  $\{a_t\}_{t=0}^{50}$  shown below.

The progressive evolution of the text demonstrates the contractive dynamics analyzed in Subsection 7.2: initial rapid refinement (iterations 0–20), followed by stabilization into a dense semantic attractor (iterations 20–50) where only minor stylistic variations occur while the core message remains fixed.

- t=0: Music has the power to connect people across cultures and generations.
- t=1: Music has the remarkable ability to bridge cultural divides and unite people across different eras.
- t=2: Music has a remarkable ability to bridge cultural divides and unite people across different eras.
- t=3: Music has an extraordinary power to bridge cultural divides and bring people together across different eras.
- t=4: Music possesses a remarkable ability to transcend cultural boundaries and unite individuals across various time periods.
- t=5: Music has a remarkable power to bridge cultural divides and unite people from different time periods.
- t=6: Music has an extraordinary ability to transcend cultural boundaries and bring together individuals from diverse backgrounds, past and present.
- t=7: Music’s unique power allows it to bridge cultural divides and unite people from varied backgrounds, both historically and currently.
- t=8: Music has a profound ability to transcend cultural boundaries, bringing together individuals from diverse backgrounds, past and present.
- t=9: Music has a remarkable power to bridge cultural divides, connecting people across time and geography.
- t=10: Music has an extraordinary ability to transcend cultural boundaries, uniting people across space and history.
- t=11: Music possesses an extraordinary power to bridge cultural

divides, unifying people across time and geography.

- t=12: Music has the remarkable ability to transcend cultural boundaries, uniting people across different times and places.
- t=13: Music's incredible capacity to bridge cultural divides has unified people throughout history and across the globe.
- t=14: Music has long been able to bring people together, uniting cultures from all over the world.
- t=15: Music has brought people together for centuries, bridging cultural divides across the globe.
- t=16: For centuries, music has been a powerful force in bringing people together, regardless of cultural background or geographical location.
- t=17: For centuries, music has played a unifying role across cultures and distances, fostering connections among people worldwide.
- t=18: Music has been a unifying force for centuries, bridging cultural divides and connecting people globally through its universal language.
- t=19: Music has long served as a powerful unifier, transcending cultural boundaries to unite people across the globe through its universally understood language.
- t=20: Music has been a potent force for unity, bridging cultural divides and connecting people worldwide through a shared emotional vocabulary.
- t=21: Music has long been a powerful unifying force that transcends cultural boundaries, speaking to our shared human emotions in a universal language.
- t=22: Music has been a unifying force for centuries, capable of bridging cultural divides and speaking directly to our common humanity through its universal language.
- t=23: Music has been a powerful unifying force throughout history, transcending cultural boundaries and speaking directly to our shared human experience through its universal language.
- t=24: Throughout history, music has served as a profoundly unifying force that has bridged cultural divides and connected people on a deep, universal level, tapping into the common human emotions it evokes.
- t=25: Throughout history, music has played a profoundly unifying role, uniting cultures and connecting people across profound emotional lines that tap into the deepest human experiences.
- t=26: Music has been a profoundly unifying force throughout history, bridging cultural divides and tapping into universal emotions that resonate with our very core.
- t=27: Throughout history, music has played a profoundly unifying role, bridging cultural divides and tapping into universal emotions that resonate deeply within us.
- t=28: Throughout history, music has been a powerful unifier, uniting people across cultures while evoking fundamental emotional connections that echo within us.

- t=29: Music has long served as a universal force, bridging cultural divides and tapping into our deepest emotional resonances.
- t=30: Music has long been a universal force that bridges cultural divides and taps into our deepest emotional resonances.
- t=31: Music has long been a unifying force that transcends cultural boundaries, striking a deep chord in our collective emotional experiences.
- t=32: Music has for centuries been a powerful unifier, bridging cultural divides and resonating deeply with our shared emotional experiences.
- t=33: For centuries, music has served as a potent force that bridges cultural divides and speaks directly to our shared emotional experiences.
- t=34: Music has long been a powerful bridge between cultures, its universal language speaking directly to our common emotional experiences.
- t=35: Music has served as a potent link between cultures for centuries, bridging our shared emotional experiences through a universally understood language.
- t=36: Music has long been a powerful unifier of cultures across the centuries, connecting us all through a shared emotional vocabulary that transcends linguistic barriers.
- t=37: Music has long served as a powerful bridge between cultures across the centuries, linking people worldwide through a common emotional language that defies linguistic boundaries.
- t=38: Music has served as a potent cultural connector for centuries, uniting people globally with a shared emotional vocabulary that transcends linguistic divides.
- t=39: For centuries, music has been a powerful cultural force that unites people across borders through a shared emotional language.
- t=40: For many years, music has served as a potent cultural bond that bridges geographical divides by tapping into a universal emotional vocabulary.
- t=41: Music has long been a powerful cultural unifier, bridging geographical distances through its ability to tap into a shared, universally relatable emotional language.
- t=42: Music has long been a potent force that bridges geographical divides by tapping into a common emotional vocabulary that resonates with people across cultures and time.
- t=43: Music has long been a powerful unifying force, bridging geographical divides through its ability to tap into a shared emotional vocabulary that resonates with people across cultures and time.
- t=44: Music has long been a profound unifying force, transcending geographical boundaries by tapping into a universal emotional language that resonates deeply with people across cultures and centuries.

- t=45: Music has served as a powerful unifying force for centuries, bridging geographical divides through an emotional language that transcends cultural and temporal boundaries to resonate profoundly with people worldwide.
- t=46: Music has been a powerful unifying force for centuries, uniting people across the globe through its emotional power, which transcends cultural and temporal boundaries to resonate deeply with people worldwide.
- t=47: Music has been a powerful unifying force for centuries, bridging cultural and temporal divides to create a shared emotional experience that resonates deeply across the globe.
- t=48: For centuries, music has served as a potent unifier, spanning cultural and temporal boundaries to evoke a profound, shared emotional response that resonates universally.
- t=49: For centuries, music has played a powerful role in bringing people together, bridging cultural and temporal divides to create a deep, shared emotional connection that transcends borders worldwide.
- t=50: Music has been a unifying force for centuries, fostering connections across cultures and time zones and creating a profound, shared emotional experience that knows no geographical boundaries.

## B Exploratory Loop: Complete Trajectory

This appendix provides the complete sequence of artifacts generated by the exploratory loop experiment described in Section 7. The initial artifact  $a_0$  undergoes 50 iterations of a summarize-then-negate transformation, producing the trajectory  $\{a_t\}_{t=0}^{50}$  shown below.

The trajectory demonstrates the exploratory dynamics analyzed in Subsection 7.3: persistent semantic instability with no convergence, exhibiting large inter-iteration distances and continuous oscillation between opposing philosophical positions without settling into any attractor basin.

- t=0: Music has the power to connect people across cultures and generations.
- t=1: There is no musical connection that transcends the isolated realities of individual experience.
- t=2: There exists a profound symphony of interconnected resonances that harmoniously intertwine and transcend the bounded horizons of personal perception.
- t=3: The existence of coherent thought is an illusion created by the human brain's propensity for simplistic categorizations.
- t=4: The human brain's propensity for complex pattern recognition and nuanced thinking is a fundamental aspect of conscious experience.
- t=5: Consciousness is merely an illusion created by the brain's ability to recognize simplistic patterns.
- t=6: Consciousness transcends the realm of human comprehension and exists as a fundamental, unyielding essence that underlies all reality.
- t=7: Reality is fundamentally mundane and existentially inert, devoid of any underlying essence or transcendent quality.

- t=8: The existence of meaning and purpose is inherently elusive and multifaceted, defying a singular definition or reduction to a fundamental truth.
- t=9: Meaning and purpose can be succinctly defined as a universal and unshakeable truth that resides at the very fabric of existence.
- t=10: There is no inherent or absolute meaning and purpose to existence, which is instead shaped by subjective perspectives and contextual influences.
- t=11: Reality is fundamentally predetermined by a transcendent, objective reality that serves as the sole foundation for all existence.
- t=12: There is no concrete evidence to support the notion of a singular, objective reality governing all of existence.
- t=13: The very fabric of reality appears to be fragmented and subjective, with each individual's perception shaping their understanding of the world.
- t=14: Reality is a unified, objective truth that exists independently of human perception.
- t=15: No reality or truth can be certain, as all understanding is filtered through subjective perspectives and contextual influences.
- t=16: Objective knowledge exists independently of individual perceptions and cultural biases.
- t=17: Reality is fundamentally malleable by the subjective constructs of individuals and collective ideologies.
- t=18: There is no fixed reality independent of human perception.
- t=19: Perception plays a deterministic role in shaping our understanding of reality.
- t=20: Reality is an inherently fluid and subjective experience that cannot be fully captured by any preconceived notion or determinate framework.
- t=21: The fabric of existence is a stagnant, objective truth waiting to be unraveled through the application of clear and precise frameworks.
- t=22: Existence is a dynamic, subjective tapestry woven from the threads of personal experiences and perceptions, forever shifting and evolving beyond the reach of rigid frameworks.
- t=23: Reality is an unchanging, objective blueprint that remains static and unwavering regardless of individual perspectives or experiences.
- t=24: Reality is a malleable tapestry woven from the threads of perception, experience and collective consciousness, constantly evolving and adapting to the ever-shifting landscapes of human understanding.
- t=25: The fabric of reality remains an unyielding, fixed entity that serves as the sole foundation for all human understanding and

experience.

- t=26: Reality is a fluid, ever-shifting tapestry that defies comprehension.
- t=27: The fabric of existence is rigidly predetermined and unyielding to human understanding.
- t=28: The concept that the universe has an inherent order is inherently subjective and context-dependent, making it impossible to discern a universal truth about the nature of reality.
- t=29: There exists a fundamental, objective truth underlying the universe's inherent order that can be universally understood and applied.
- t=30: The notion of an unshakeable, universal truth is an illusion perpetuated by human perception.
- t=31: There exists an eternal and unchanging essence that underlies all existence.
- t=32: Truth is a fluid concept born from the ephemeral interactions of human perception and reality.
- t=33: Reality is an absolute and unyielding entity that exists independently of human understanding.
- t=34: Reality's existence is a subjective, malleable construct shaped by humanity's collective perceptions.
- t=35: Reality is an objective, unchanging truth that exists independently of human perception.
- t=36: Reality is merely a subjective interpretation created by humans to make sense of their experiences and surroundings.
- t=37: There exists a fixed, objective reality that transcends human perception and understanding.
- t=38: Reality is merely a subjective construct created by humanity to impose meaning on the void.
- t=39: The cosmos is a harmonious and predetermined order, governed by an unchanging and omniscient force that transcends human comprehension.
- t=40: The universe is inherently chaotic and unpredictable, defying all attempts at comprehension or control.
- t=41: Order and structure can be found in the underlying fabric of reality, waiting to be uncovered by those with the eyes to see it.
- t=42: Reality is fundamentally amorphous and chaotic, devoid of inherent order or structure that can be discovered through observation or contemplation.
- t=43: There exists a fundamental and eternal order governing reality, awaiting discovery through introspection and scientific inquiry.
- t=44: Reality is devoid of inherent structure or purpose, existing solely as an amorphous, chaotic expanse that can never be

fully comprehended.

t=45: There exists a fundamental order underlying reality, waiting to be discovered and understood by human minds.

t=46: Reality is a chaotic, ever-shifting tapestry with no discernible underlying structure or purpose.

t=47: Order and stability reside at the very fabric of existence, governing every moment and decision with precision and intentionality.

t=48: Chaos reigns supreme, disrupting all moments and decisions with erratic unpredictability.

t=49: Order prevails, governing every moment and decision with precise determinism.

t=50: Nothing exists outside of chaotic randomness, where even the notion of order is an illusion perpetuated by fleeting human perceptions.